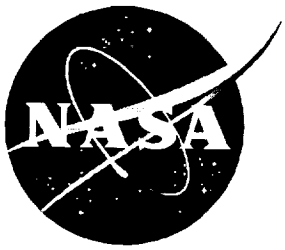

NASA Contractor Report 4650

An Assessment of Viscous Effects in Computational Simulation of Benign and Burst Vortex Flows on Generic Fighter Wind-Tunnel Models Using TEAM Code

Tim A. Kinard, Brenda W. Harris, and Pradeep Raj
Lockheed Aeronautical Systems Company • Marietta, Georgia

National Aeronautics and Space Administration
Langley Research Center • Hampton, Virginia 23681-0001

Prepared for Langley Research Center
under Contract NAS1-19000

March 1995

This publication is available from the following sources:

NASA Center for AeroSpace Information
800 Elkridge Landing Road
Linthicum Heights, MD 21090-2934
(301) 621-0390

National Technical Information Service (NTIS)
5285 Port Royal Road
Springfield, VA 22161-2171
(703) 487-4650

TABLE OF CONTENTS

AN ASSESSMENT OF VISCOUS EFFECTS IN COMPUTATIONAL SIMULATION OF BENIGN AND BURST VORTEX FLOWS ON GENERIC FIGHTER WIND-TUNNEL MODELS USING TEAM CODE

Tom A. Kinard
Brenda W. Harris
Pradeep Raj

Lockheed Aeronautical Systems Company

SUMMARY

Vortex flows on a twin-tail and a single-tail modular transonic vortex interaction (MTVI) model, representative of a generic fighter configuration, are computationally simulated in this study using the Three-dimensional Euler/Navier-Stokes Aerodynamic Method (TEAM). The primary objective is to provide an assessment of viscous effects on benign (10° angle of attack) and burst (35° angle of attack) vortex flow solutions. This study was conducted in support of a NASA project aimed at assessing the viability of using Euler technology to predict aerodynamic characteristics of aircraft configurations at moderate-to-high angles of attack in a preliminary design environment. The TEAM code solves the Euler and Reynolds-averaged Navier-Stokes equations on patched multiblock structured grids. Its algorithm is based on a cell-centered finite-volume formulation with multistage time-stepping scheme. Viscous effects are assessed by comparing the computed inviscid and viscous solutions with each other and with experimental data. Also, results of Euler solution sensitivity to grid density and numerical dissipation are presented for the twin-tail model. The results show that proper accounting of viscous effects is necessary for detailed design and optimization but Euler solutions can provide meaningful guidelines for preliminary design of flight vehicles which exhibit vortex flows in parts of their flight envelope.

INTRODUCTION

Advanced fighter aircraft must be designed to meet stringent performance requirements over a wide range of angle-of-attack and Mach number conditions. The design process can be greatly helped if aerodynamic characteristics associated with vortex-dominated flows at moderate to high angles of attack can be simulated in an *accurate*, *cost-effective* and *timely* manner using computational fluid dynamics (CFD). In late 1993, NASA-Langley Research Center (LaRC) undertook a study aimed at assessing the viability of using current Euler CFD technology (CFD methods that solve the inviscid, nonlinear Euler equations) to predict these characteristics from a preliminary design perspective. A team consisting of LaRC, Lockheed Aeronautical Systems Company (LASC), Lockheed Fort Worth Company (LFWC), and Boeing Defense and Space Group (BDSG), was formed to support this study. Each participant was tasked with assessing one of the four codes representing four distinct current state-of-the-art numerical techniques. LASC was assigned the patched multiblock structured-grid TEAM code [1,2], BDSG used the OVERFLOW code [3] based on overset multiblock structured grids, LFWC employed their Cartesian unstructured-grid SPLITFLOW code [4], and LaRC used the USM3D code [5] based on tetrahedral unstructured grids.

The initial plan called for each code to be exercised on two modular transonic vortex interaction (MTVI) models, one single tail and the other twin tail, with the part-span leading-edge flap deflected down 30°. Computed forces, moments, and surface pressures at 0.4 Mach number and a range of pitch and side-slip angles were to be correlated with experimental data obtained previously by LaRC from a 7' x 10' wind-tunnel test. Grid sensitivity and wall-interference effects were to be addressed for a few selected cases. Also, data on computer resource requirements, problem set up time, etc., were to be compiled for each code.

Upon further examination, the patched multiblock structured grid technology assessment task (involving TEAM application and assigned to LASC) was revised. Its focus was shifted to assessing viscous effects for one benign ($\alpha = 10^{\circ}$) and one burst ($\alpha = 35^{\circ}$) vortex-flow case on the baseline (undeflected flap) twin-tail and single-tail MTVI models. This refocusing was prompted by the fact the use of patched multiblock structured-grid Euler technology represented by the TEAM code entails relatively long turnaround times that are incompatible with the levels needed to meet cost and schedule constraints of a typical preliminary design exercise. The desirable levels range from a few hours to a day. Without rapid turnaround, a CFD method cannot be fully effective in a preliminary design environment. Patched multiblock grid generation about aircraft configurations can typically take anywhere from a few days to a few weeks contributing to the long turnaround times. However, patched multiblock flow solvers have been extensively used for both inviscid [6-8] and viscous [9-11] flow computations resulting in a better understanding of their capabilities as compared to the unstructured-grid solvers. Therefore, it was decided to use TEAM to determine the implications of neglecting viscosity on the Euler solutions to be generated under the present project.

In this report, computed solutions obtained using the TEAM code are compared with the available experimental data [12] for two MTVI models. Note that the primary emphasis is on assessing the viscous effects. Comparisons of forces and moments are presented in a tabular form. Plots of surface pressure correlations are presented for six cross-flow stations, three on the forebody and the rest on the aft-fuselage and wing. A limited amount of computed off-body flow-field data is also included. In addition, convergence histories and data on computer resources are presented. The report concludes with suggestions for future work.

LIST OF SYMBOLS

b	span
c	mean aerodynamic chord
CFL	Courant-Friedrichs-Lewy number
C_p	coefficient of pressure
C_D	drag coefficient
C_L	lift coefficient
C_m	pitching-moment coefficient
M	free-stream Mach Number
Re	Reynolds number
S_{ref}	reference area
x,y,z	body-fixed Cartesian coordinate system: x positive along model axis, y positive from symmetry plane to wing tip (starboard), and z positive up
α	angle of attack

ANALYSIS TOOLS

In this section, software and hardware tools used in the present investigation are outlined; solutions obtained through the application of these tools are presented in the following sections. These tools were required to generate grids, produce flow solutions, and postprocess the solutions to extract the desired aerodynamic data. The grid-generation and postprocessing tasks were carried out on a graphics workstation and the solutions were produced on a supercomputer.

The analysis process started with the configuration geometry files which were supplied by NASA [12] and used as input for grid generation. The GRIDGEN, Version 8, code [13], a product of MDA Engineering, Inc., was used to produce all multiblock, structured grids for this investigation. The code was run on Silicon Graphics, Inc., IRIS 4D/35 graphics workstation. GRIDGEN allows a user to create boundary-condition datasets interactively as a part of the grid generation process. These datasets define the appropriate conditions to be imposed on the boundaries of a block, such as solid, far field, etc., and are required to execute the TEAM, Version 713, flow solver [2] used here. The flow solver was run on the Cray Research, Inc., C-90 supercomputer of the NASA Numerical Aerodynamic Simulator (NAS) facility. The FAST code [14] and Tecplot, a product of Amtec Engineering, Inc., were used to postprocess the flow solutions in order to generate the desired on and off-body flow quantities. The ACE/gr software package [15] was the primary tool for producing x-y type plots such as convergence histories and surface pressure correlations.

All software and hardware tools mentioned above have been adequately described in available literature. Therefore, their descriptions will not be repeated here. Appropriate references are cited above for those readers interested in more details.

MTVI TWIN-TAIL MODEL

The analysis of MTVI twin-tail model is discussed in this section. Details of grid generation and flow solutions are presented below. Both inviscid and viscous computations are performed for the benign and burst vortex flow conditions. Also, an attempt is made to simulate the effect of leading-edge flap deflection using the surface transpiration boundary condition [16] option in TEAM.

Geometry

A perspective view of the surface geometry of this model is shown in figure 1. The model has a chined forebody with an included angle of 100° and a cropped-delta wing with a leading-edge sweep of 60° and an aspect ratio of approximately 1.8. The entire configuration is made up of analytically defined components. The wing airfoil section is biconvex whereas the vertical-tail section is a thin diamond shape. All edges of the wing and tail surfaces are sharp.

We used a pointwise definition of the surface supplied by NASA-LaRC in plot3D format. NASA generated the pointwise definition from the analytical definition on a Cray computer using double precision. Since Cray double precision is 64 bit accurate, there were some twenty digits after the decimal point. Since a workstation with 8 bit words was used for grid generation, the data were appropriately truncated down to seven digits past the decimal point. Care was taken to ensure that the truncated data matched the corresponding significant digits in the original dataset.

Grid Generation

The GRIDGEN software package was used to generate grids for both inviscid and viscous analyses. An O-H topology was chosen for domain decomposition. This topology is a good compromise between the O-O and H-H topologies. The O-O topology is most efficient as far as grid distribution is concerned but is somewhat more cumbersome to implement. Grids of H-H topology are easier to generate than O-O type but many more grid points are required to obtain comparable resolution. The use of O-H topology introduced a pole boundary—singular line emanating from the nose—into the flow field that posed some difficulties in the intial stages of the flow analysis as discussed in the following section.

Inviscid grid

A grid with 16 blocks and nearly 1.9 million nodes was generated around the twin-tail MTVI model in approximately eight days. A general representation of the layout of the blocks is shown in figure 2. Grids on the six faces of each block were created using the algebraic transfinite interpolation (TFI) option. Excessive grid skewness on certain faces was removed by exercising the elliptic smoothing option. The volume grid was generated from the input faces using TFI. Negative volumes, if any, were removed by running an elliptic smoother on the "bad" zones. The block interfaces (where two neighboring blocks abut) were constructed to have identical distribution of nodes on both sides. This was a constraint imposed by GRIDGEN, Version 8; the TEAM flow solver itself could accommodate grids with or without point-to-point match interfaces.

Initial attempts at running the TEAM flow solver with the grid containing a

pole boundary caused it to diverge unless the input CFL number was reduced much below the "standard" value of 6. It was observed that the maximum residual was on or near the pole boundary. In an attempt to rectify this problem, the block structure near the nose was modified as shown in figure 3 to eliminate the pole boundary. This modification solved the divergence problem, but the surface pressure contours near the nose exhibited discontinuities which were traced to the poor quality of the grid in this region. The grid distribution was not smooth and could not be improved due to the constraints imposed by the new block structure. The solutions in the region near the nose were of questionable quality. It was also realized that generating refined grids for viscous analysis would further degrade the grid quality. Consequently, the use of modified grid (without pole boundary) was abandoned. Instead, the treatment of boundary condition for pole boundaries in the flow solver was modified along the lines of the CFL3D [17] code. This change allowed the solver to converge on the original grid even when the standard CFL number was used. All subsequent analysis was done using grids with a pole boundary. A coarser grid was also generated by reducing the grid density to facilitate evaluation of solution sensitivity to grid size. The coarser grid was topologically identical to the fine grid but contained only about 1.1 million nodes.

Viscous grid

With the knowledge gained from the Euler grid, a viscous grid was generated. We took advantage of a feature of GRIDGEN, Version 8, that allows the dimensions of the grid system to be updated in a semiautomatic manner. The user changes the number of points on an edge and this change propagates to other blocks automatically. Sometimes the code cannot automatically determine the number of points on another edge, the user is then prompted for an input and the process

continues until a balanced system is obtained. This procedure was applied to the Euler grid. Once a balanced system was obtained, the point distribution on some of the edges was changed to cluster grids near solid surfaces and wakes as needed to solve the thin-layer RANS equations. A spacing of 0.0001 grid units was used for the first cell off the surface. After the distributions were set for all block faces, the volume grid was generated using TFI. Elliptic smoothing was then used to remove any cells with negative volumes, or excessively skewed or crossed cells. The resulting grid had approximately 2.2 million nodes.

Grid quality

The grids generated in the manner described above were of good enough quality for Euler analysis. However, difficulties were initially experienced with viscous analysis which failed to converge at standard CFL numbers of 3 to 4 even though care was taken to ensure that the grid contained no cells with negative volumes or high levels of skewness. An additional check of other grid-quality measures was then made by analyzing the grid using Qbert [18] which generates statistics on aspect ratio and truncation error. The truncation error estimate is for central difference solvers like TEAM.

The output from Qbert contains an average and a sigma, standard deviation, for both the aspect ratio and truncation error. For an ideal grid, the aspect ratio of the cells should be unity which corresponds to the cells being perfect cubes. The user should strive to make the average plus the sigma value as close to unity as practical. The closer the aspect ratio is to unity the faster the code will converge. Conversely, the farther the aspect ratio is from unity the slower the code will converge, or in the worst case the code will not converge. This grid-quality measure is suitable for inviscid grids but not for viscous grids which by design contain highly

elongated cells with high aspect ratios. For such grids, only the truncation error measure can be used.

The ideal value of the average plus sigma of the truncation-error measure is zero. The higher the value, the higher the dissipation of the grid and more incorrect the flow solution. As a general rule, if the sum of the average and sigma is less than one, the grid may be considered *very good*. For values between one and five, the grid may be considered *good*. The grid is *average* for values between five and ten, and above ten the grid is considered *poor*. (Note that the truncation error reported in Qbert should be multiplied by the second derivative of the flow solution to yield the true solution error.) On the truncation-error basis, the viscous grids were found to be of poor quality. The quality was improved through redistribution and elliptic smoothing and many of the difficulties in running the code were alleviated.

Benign Vortex Flow

The benign vortex flow case corresponding to 0.4 Mach number and 10.1° angle of attack is the first case to be examined in this report. Two vortices are present in the flow field. The first one emanates from the chine on the forebody and travels down the body on the leeward side. The second vortex results from flow separation along the sharp leading edge of the wing and travels downstream along the wing leading edge towards the tip. Results of TEAM analysis are presented in this section.

Euler solutions

The first Euler solution was produced on the fine grid containing 16 zones

and 1.9 million nodes. The surface pressures near the chine on the forebody exhibited wiggles which were caused by a grid that was too sparse in the vicinity of the chine to adequately resolve high gradients. The surface grid on the forebody was redistributed by moving more points to the chine area and a new volume grid was generated which largely eliminated the wiggles. For this analysis, the entire computational domain was initialized to the free-stream conditions and the numerical parameters were set to the following values: four stages for the pseudo-time marching scheme with one evaluation of dissipation, CFL number of 6, variable-coefficient implicit residual smoothing, and modified adaptive dissipation (MAD) scheme with VIS2 = 0.25 and VIS4 = 2.5. The solution took approximately 12.7 seconds per cycle and 46 megawords (MW) of memory on the Cray C-90 supercomputer. This translates to the code performance of 7 μs (microseconds) of CPU time per node per cycle and 25 words of memory per node point. (The memory requirement in terms of words per node changes somewhat with the number of blocks and/or distribution of nodes among the blocks.)

Figure 4 shows plots of convergence histories for this case. More than four orders of magnitude reduction in average residual was obtained in 1500 cycles. The convergence histories of lift, drag and pitching moment coefficients show that the values were well converged in about 1000 cycles. The final values of the forces and moments are compared with the test data in table 1. The TEAM Euler solutions underpredict the lift and moment and overpredict drag. Note that the C_D values (for Euler solution) shown in the table include a C_{Do} of 0.02. The grey-shaded surface pressure distribution on the upper and lower surfaces is shown in figure 5. On the upper surface, the footprint of the vortices and the interaction between the wing vortex and vertical tail are clearly visible.

Correlations of computed surface pressure with experimental data at six cross-flow stations shown in figure 6 are presented next. Results for three stations

on the forebody are shown in figure 7 and for three stations on the aft-fuselage and wing are in figure 8. Since the surface gridlines were not aligned with any of these stations, computed surface pressures were interpolated to obtain the data shown in these figures. (Note that the vertical scales are different between the two figures.) The lower surface pressures agree well with the test data on the three forebody stations where lower surface pressure data was available. Discrepancies between the computed solutions and experimental data are clearly visible on the upper surface.

Grid sensitivity

In order to assess the sensitivity of the solution to grid density, solutions on the fine grid were compared with those on a coarser grid which was topologically identical to the fine grid but contained only 1.1 million nodes. The forces and moments are compared in table 2 and the surface pressures are compared in figures 9 and 10. It is clear from these comparisons that the coarse grid did not offer adequate flow resolution. However, a definite conclusion could not be made about the adequacy of the finer grid without additional analyses. The schedule and resource (labor hours and computer hours) constraints did not permit that.

It may, however, be conjectured that the fine grid is probably not totally adequate. This is based on past experience with vortex-flow analyses using TEAM as well as the single-tail MTVI results which show that Euler solutions usually overpredict the lift coefficient. In contrast, data in table 2 shows that the computed value of lift for the present fine grid is *less* than the experimental value. The most likely cause is a lack of grid resolution, especially on the aft part of the wing. We recommend that this issue be resolved through additional computations.

Numerical dissipation effect

The TEAM code contains several artificial dissipation schemes. For many transonic-flow Euler computations, a flux-limited adaptive dissipation (FAD) scheme has been successfully used. Although the modified adaptive dissipation (MAD) scheme is considered the least dissipative, transonic-flow solutions have not shown a large sensitivity. In order to assess the sensitivity of MTVI vortex flows to each scheme, Euler solutions were generated using both FAD and MAD on the same grid. Both solutions were run to the same level of convergence. Pressure coefficients were extracted at the six cross-flow stations where test data was available. A comparison between the two solutions shown in figure 12 illustrates the numerical dissipation effect. The higher dissipation of the FAD scheme produces solutions that underpredict vortex strength and move the vortex core further inboard. This comparison clearly shows that the MAD scheme is less dissipative of the two, and therefore is the logical choice for viscous analysis where the effects of numerical dissipation must be kept to a minimum. Consequently, the MAD scheme has been used for all analyses, Euler as well as RANS, reported here unless noted otherwise.

Simulated flap deflection

As mentioned in the Introduction section, the present study involved only baseline MTVI models, i.e., all flaps in the retracted position. An attempt was made to simulate the effect of deploying the part-span leading-edge flap down by 30° using the surface transpiration feature in TEAM. A solution was obtained by restarting from the baseline solution and applying the transpiration boundary condition on the cells defining the flap. Convergence histories are shown in figure 13 from the point of the restart. Although the computed results show a reduction in

lift and drag that is expected for this case where the leading-edge flap is deflected down and is confirmed by the experimental data, the magnitude of change from the baseline to the deflected case is not accurately predicted by the present simulation. The computed and measured surface pressure distributions in figures 14 and 15 also show poor agreement. In light of other applications of the surface-transpiration feature, further study is required before concluding that it is not effective to accurately model the problem in question.

Viscous effects

The approach to assessing the viscous effects involved comparing Euler solutions with thin-layer RANS solutions. The RANS solutions were obtained for the same flow conditions as the Euler, i.e., 0.4 Mach number and 10.1° angle of attack, but using the viscous grid. The Reynolds number based on the mean aerodynamic chord was 2.7 million and the turbulence model was the standard Baldwin-Lomax model [19]. The numerical parameters for this analysis were: 4 stage scheme with 2 evaluations of dissipation, a CFL number of 3, MAD scheme with VIS2 = 0.25 and VIS4 = 2.0. Over three orders of magnitude reduction in residual was achieved in 3000 cycles as shown in figure 16. Note that more cycles were needed to get a converged solution than used for Euler. The solution took approximately 27.7 seconds per cycle and 64 megawords (MW) of memory on the Cray C-90 supercomputer. This translates to the code performance of 13 μs (microseconds) of CPU time per node per cycle and 30 words of memory per node point.

Surface pressure data was extracted at the same six stations used in correlating the Euler solutions. A close examination of the data showed that the standard Baldwin-Lomax turbulence model was too dissipative and therefore failed to accurately capture the vortex off the chine. The Baldwin-Lomax model was then

modified to include the Degani-Schiff modification [20]. The solution was restarted using the modified turbulence model and additional cycles were executed. The corresponding convergence histories are shown in figure 16.

The grey-shaded surface pressure distribution on the upper and lower surfaces is shown in figure 17. The force and moment values are compared with experimental data (as well as the Euler results) in table 1. The source of discrepancy is most likely the grid coarseness. Many features of this complex vortical flow were not captured in sufficient detail as indicated by the correlations of surface pressures in figures 18 and 19. Also, the upper-surface pressure distribution curve at x = 14.5 resulting from the TEAM viscous analysis exhibits a kink near the peak. Preliminary investigation shows that the presence of a block boundary at this location is the most probable cause. Further study is required to precisely identify the cause and rectify it.

From these results, it may be surmised that this benign vortex flow on the MTVI twin-tail model exhibits noticeable viscous effects. The forces and moments predicted by the Euler solutions may be acceptable for preliminary design studies. But the solutions are not well suited for a detailed design or optimization study due to discrepancies between the computed and measured surface pressure distributions. Further investigations are needed to more accurately assess the viscous effects.

Burst Vortex Flow

The burst vortex case corresponds to a flow condition where the Mach number is 0.4 and the angle of attack is 35.21°. At this flow condition the vortex does not retain its cohesive structure as in the benign vortex case at lower α. Also, the flow field in the burst region above the wing is unsteady.

Euler solution

The flow field from the benign vortex case was used as an initial condition for this analysis, i.e., solution for the $\alpha = 35.21^{\circ}$ case was generated by restarting from the $\alpha = 10.1^{\circ}$ solution. No changes were made to the numerical parameters and additional cycles were performed. The residual histories in figure 20, when contrasted with those in figure 4, clearly show a lack of convergence. The residual drops by nearly two orders of magnitude and then stalls. The forces and moments also exhibit fluctuations about a "mean" value. Visualization of the flow field at cross plane stations illustrates the cause of this behavior: the forward stations show coherent vortex structures whereas the aft ones show burst vortex flow. The grey shaded surface pressure distribution in figure 21 also bears it out. The computed mean values of force and moment coefficients are compared with the test data in table 3.

Viscous effects

The viscous analysis of burst vortex case was more difficult to perform than that of the benign case. The first attempt at generating a solution was made by restarting from the viscous benign case solution. This worked well for several hundred cycles but unusually high residuals were generated near the vertical tail which ultimately caused the solution to diverge. After examining the grid in this area, minor changes were made to grid distributions near the tail and additional elliptic smoothing was performed which further improved the grid quality. The solution then proceeded without any difficulty and an additional 3000 cycles were carried out.

The residual histories in figure 22, when contrasted with those in figure 16, clearly reflect the unsteady nature of this flow. The residual drops by nearly two orders of magnitude and then stalls. The forces and moments exhibit fluctuations about a "mean" value. The computed mean values of force and moment coefficients are compared with test data in table 3. The grey shaded surface pressure distribution in figure 23 shows significantly lower levels of $-C_p$ for the footprint of the vortices on the aft portions of the model. The normalized total pressure distributions at six cross-flow planes in figures 24 and 25 clearly illustrate the cause of this behavior: the three forebody locations show a well-defined chine vortex, the fourth location shows a well-defined wing vortex and a diffused chine vortex, and the last two show merging and coalescing of vortices leading to a very diffused distribution of total pressure.

Computed surface pressure distributions at six cross-flow stations are compared with the test data as well as Euler solutions in figures 26 and 27. The viscous solutions are in good agreement with test data except for the most forward station. The two probable causes for this discrepancy are: (1) lack of convergence of the solution near this stations where the cells are relatively small, and (2) the grid density and/or distribution may not be adequate to accurately capture the gradients. Further studies are needed to resolve this issue. Unlike the benign vortex flow case, this case exhibits much stronger viscous effects especially on the forebody region where the Euler solutions deviate substantially from the experimental values. Interestingly, computed solutions correlate well in the burst vortex region in both trends and magnitudes.

MTVI SINGLE-TAIL MODEL

The analysis of MTVI single-tail model is discussed in this section. Details of grid generation and flow solutions are presented below. Both inviscid and viscous computations are performed for the benign and burst vortex flow conditions. The flow conditions are nearly identical to those for the twin-tail model.

Geometry

A perspective view of the surface geometry of this configuration is shown in figure 28. The wing and fuselage geometries are identical to those of the twin-tail model described on page 6. We used a pointwise definition of the surface geometry supplied by NASA-LaRC in the plot3D format. The pointwise definition was generated from the analytical definition of the geometry on a Cray computer using double precision. Just like the twin-tail model, the data were truncated before using them to generate grids. (See page 6 for a discussion of the truncation process.)

Grid Generation

The GRIDGEN software package was used to generate grids for both inviscid and viscous analyses. The approach was very similar to that used for the twin-tail model. However, a slightly different topology was selected in an attempt to improve grid quality by reducing skewness. The grid was of an H-H topology between the plane of symmetry and the wing tip and an O-type grid (outboard of the tip) connected the upper and lower-surface blocks.

Inviscid grid

A grid with 16 blocks and nearly 1.9 million nodes was generated around the single-tail MTVI model in approximately eight days. A general representation of the layout of the blocks is shown in figure 29. Grids on the six faces of each block were created using the algebraic transfinite interpolation (TFI) option. Any grid skewness on the faces was easily removed by exercising the elliptic smoothing option. The volume grid was generated from the input faces using TFI. Negative volumes, if any, were removed by running an elliptic smoother on the "bad" zones. The block interfaces (where two neighboring blocks abut) were constructed to have identical distribution of nodes on both sides.

Viscous grid

The viscous grid was generated by adding points in the direction normal to the surface and then clustering them closer to the surface. The number of points on the wing surface essentially remained unchanged, whereas the number of points on the body was increased due to grid clustering normal to the vertical tail. The dimensions of the grid system were updated in a manner identical to that used for the twin-tail case (see page 8). The Euler grid was enriched and the point distribution on some of the edges was changed to cluster grids near solid surfaces and wakes as needed to solve the thin-layer RANS equations. A spacing of 0.0001 grid units was used for the first cell off the surface. After the distributions were set for all block faces, the volume grid was generated using TFI. Elliptic smoothing was then used to remove any cells with negative volumes, or excessively skewed or crossed cells. The resulting grid had approximately 2.7 million nodes distributed among 16 blocks.

Grid quality

The experience gained from the twin-tail analysis was exploited in generating "good" quality grids for both inviscid and viscous analysis. The grid quality measures supplied by the Qbert code were used to evaluate the grids.

Benign Vortex Flow

The benign vortex flow case corresponds to 0.4 Mach number and 10.1° angle of attack. Two vortices are present in the flow field. The first one emanates from the chine on the forebody and travels down the body on the leeward side. The second vortex results from flow separation along the sharp leading edge of the wing and travels downstream along the wing leading edge towards the tip. Results of TEAM inviscid and viscous analyses are presented in this section.

Viscous effects

The approach to assessing the viscous effects was analogous to the one used for the twin-tail model. It involved comparing Euler solutions with thin-layer RANS solutions and test data.

The Euler solution was produced on the fine grid containing 16 zones and 1.9 million nodes. For this analysis, the entire computational domain was initialized to the free-stream conditions and the following numerical parameters were used: four stages for the pseudo-time marching scheme with one evaluation of dissipation, CFL number of 6, variable-coefficient implicit residual smoothing, and the MAD scheme with VIS2 = 0.25 and VIS4 = 2.5. The solution took approx. 12.6 seconds

per cycle and 46 megawords (MW) of memory on the Cray C-90 supercomputer. This translates to the code performance of 7 μs (microseconds) of CPU time per node per cycle and 25 words of memory per node point. Figure 30 shows plots of convergence histories for this case. More than four orders of magnitude reduction in average residual was obtained in 1500 cycles. The convergence histories of lift, drag and pitching moment coefficients show that the values were well converged in about 1000 cycles. The final values of the forces and moments are compared with the test data in table 4. The TEAM Euler solutions overpredicted the lift, drag and moment coefficients. Note that the C_D values (for Euler solution) shown in the table include a C_{Do} of 0.02. The grey-shaded surface pressure distribution on the upper and lower surfaces is shown in figure 31 which depicts the footprint of the vortex just inboard of the wing leading edge.

The RANS solutions were obtained for the same flow conditions as the Euler, i.e., 0.4 Mach number and 10.1° angle of attack, but using the viscous grid. The Reynolds number was 2.7 million and the Baldwin-Lomax turbulence model with Degani-Schiff modification was used. The numerical parameters for this analysis were: 4 stage scheme with 2 evaluations of dissipation, a CFL number of 3, MAD scheme with VIS2 = 0.25 and VIS4 = 2.0. Over three orders of magnitude reduction in average residual was achieved in 2000 cycles as shown in Figure 32. Note that more cycles were needed to get a converged solution than used for Euler. The solution took approximately 33.5 seconds per cycle and 81 megawords (MW) of memory on the Cray C-90 supercomputer. This translates to the code performance of 13 μs (microseconds) of CPU time per node per cycle and 30 words of memory per node point. The grey-shaded surface pressure distribution on the upper and lower surfaces is shown in figure 33 which shows that the wing vortex footprint is further inboard as compared to the Euler solution in figure 31. The force and moment values are compared with experimental data and Euler results in table 4. They

agree quite well with the test data.

Surface pressure data was extracted at the six cross-flow stations shown in figure 6. Correlations of computed and measured data are shown in figures 34 and 35. For all stations, the viscous solutions are closer to the test data than the Euler solutions. The viscous solutions predict the C_p peak location quite accurately although the magnitude was underpredicted. The cause for this discrepancy needs to be investigated requiring additional computations with more refined grids as well as with a one-equation and a two-equation turbulence model.

Note that the Euler solution does not capture the chine vortex whereas a weak chine vortex was produced in the corresponding Euler solution for the twin-tail configuration. The different grid topologies on the forebody region is the most probable cause pointing to the Euler solution sensitivity to grid topology. The forebody grid was of O-H topology for the twin-tail case and of H-H topology for the single-tail case. As mentioned earlier, this change was made to reduce grid skewness on the wing surface and thereby improve overall grid quality. However, the change in topology led to the unintended effect of smearing out the forebody vortex. (Interestingly, viscous solutions for both cases produce chine vortices of comparable strength.) The Euler solution does produce a strong wing vortex whose predicted location is further outboard than that indicated by the measured data. This discrepancy results from the absence of secondary vortices which are not captured by the inviscid Euler solutions.

From these results, it may be surmised that this benign vortex flow case exhibits noticeable viscous effects. The forces and moments predicted by the Euler solutions may be acceptable for preliminary design studies. However, the Euler solutions are not well suited for a detailed design or optimization study since the surface pressure distributions clearly show relatively large discrepancies.

Burst Vortex Flow

The burst vortex case corresponds to a flow condition where the Mach number is 0.4 and the angle of attack is 35.35°. At this flow condition the vortex does not retain its cohesive structure on the aft portions of the model as in the benign vortex case at lower α. Also, the flow field in the burst region above the wing is unsteady.

Viscous effects

The approach to assessing the viscous effects was identical to that used for the benign vortex flow case, i.e., comparing Euler and viscous solutions with test data. The Euler solution was generated using the flow field from the benign vortex case as the initial condition. No changes were made to the numerical parameters and an additional 2000 cycles were performed. The residual histories in figure 36, when contrasted with those in figure 30, clearly show a lack of convergence. The residual drops by nearly one and a half orders of magnitude and then stalls. The forces and moments also exhibit fluctuations about a "mean" value. Visualization of the flow field at cross plane stations illustrates the cause of this behavior: the forward locations show coherent vortex structures whereas the aft ones show burst vortex flow. The grey shaded surface pressure distribution in figure 37 also bears it out. The computed mean values of the lift, drag, and pitching moment coefficients are compared to their measured values in table 5.

The residual histories of the RANS analysis are shown in figure 38. The benign-vortex flow field was used as the initial condition for this analysis. When contrasted with data in figure 30 for the benign vortex case, the unsteady nature of

this flow is clearly evident. The residual drops by nearly two orders of magnitude and then stalls. The forces and moments also exhibit fluctuations about a "mean" value. The grey shaded surface pressure distribution in figure 39 also illustrates the loss of a well defined footprint of the vortex, clearly visible in figure 33. The computed and measured force and moment data are presented in table 5.

Computed surface pressure distributions at six crossflow stations are compared with the test data as well as Euler solutions in figures 40 and 41. The viscous solutions are in better agreement with test data than the Euler solutions on the forebody except the most forward station. Both solutions deviate from the measured data on the aft fuselage and wing regions. The vortex bursts somewhere between the 4th and the 5th station, i.e., between x = 19.05 and 23.55. Note that the computed solutions cannot be expected to accurately represent the unsteady flow in the burst region because the pseudo-time marching procedure was employed. Interestingly, the computed solutions show the general trends of the measured data. It is not clear whether a more representative result can be obtained by averaging a set of pseudo-time solutions or whether the time-accurate solution process is required.

TAIL PLACEMENT EFFECTS

The two MTVI models considered in this study differ in only one aspect: tail placement, i.e., location of the vertical tail, as can be seen from figure 1 and figure 28. In this section, comparisons of computed solutions for both configurations are presented that highlight the effect of tail placement. Only the viscous solutions are considered in this comparison.

The effect of tail placement for the benign vortex case are shown first. On the three forebody station, there is very little change in the surface pressures as shown in figure 42. This is to be expected because of the distance separating the forebody from the tail. The differences begin to become apparent as one approaches the aft fuselage and wing stations shown in figure 43. The last two stations at 23.55 and 28.05 exhibit the largest difference. The vortex emanating from the leading edge for the single-tail case is stronger and remains further inboard when compared to the twin-tail case.

At the burst condition, a similar story emerges from the surface pressure comparisons shown in figures 44 and 45. The data on the three forebody stations agree well with each other indicating little sensitivity to tail placement. The aft-fuselage and wing stations show some differences. However, the effects cannot be assessed in any definitive manner from these results as they are just one slice of a pseudo-time marching solution of a flow that is unsteady in nature. A time-averaged result of a set of pseudo-time or time-accurate solutions is probably required to accurately assess the tail placement effects.

CONCLUSIONS AND SUGGESTIONS FOR FUTURE WORK

The results of this study contribute to assessing the viability of using current state-of-the-art Euler methods in simulating benign and burst vortex flows over sharp-edged wing-body-tail configurations. Euler inviscid and RANS viscous solutions were obtained using the TEAM code and compared with test data to develop a better understanding of the effects of neglecting viscosity when the Euler methods are applied to vortex-flow simulation. The solutions for both twin-tail and single-tail MTVI models show that

(a) care must be exercised in applying Euler technology as the solutions exhibit sensitivity to grid density, topology, and numerical dissipation, the solutions being particularly sensitive on the forebody region even though the forebody had a sharp-edge along the chine.

(b) the Euler methods successfully capture the overall features of vortex flows including vortex burst but fail to adequately model many of the details such as secondary separated flows.

(c) the integrated forces and moments as well as the overall flow features predicted by Euler methods may adequately meet the requirements of a traditional preliminary-design environment but the use of Euler methods for design optimization must be approached with caution because the distributed on and off-body flow parameters may not be of sufficient accuracy.

As is true with most research studies, the present study answered many questions and raised many new ones which could not be fully addressed due to schedule and resource constraints. We recommend that further investigation along the lines suggested below be conducted to resolve these issues:

- Both Euler inviscid and RANS viscous solutions be obtained on finer grids

than used to date to ensure that all flow features were accurately resolved. Datum solutions so obtained could be used to quantitatively evaluate the accuracy of other solutions.

- A more comprehensive analysis of the solutions generated to date be performed to examine the various on and off-body flow quantities in much more detail. The analysis would include examination of boundary-layer profiles, separation and attachment lines on the surface, skin-friction variations, location and strength of vortices, etc.
- Solutions should be obtained at other angles of attack as well as side-slip angles. The flow conditions of particular interest are those where the vortex flow transitions from benign to burst for the MTVI models. Time-accurate analysis of burst vortex flows will also be of great value in producing datum solutions.
- No study of RANS solutions is complete without investigating the effect of turbulence models on the solution. We recommend evaluating this effect by using at least a one-equation model and a two-equation model.
- The present study should be extended to assess the viability of current RANS methods to accurately predict the effect of Reynolds number difference between wind tunnel and flight on vortex flows. This is one of the key areas where CFD can fill a crucial gap in aerodynamic database for any aircraft design effort.

ACKNOWLEDGMENTS

The present study was conducted under contract no. NAS1-19000 sponsored by the Transonic/Supersonic Aerodynamics Branch, NASA-Langley Research Center, Hampton, Virginia. The LASC team would like to thank Farhad Ghaffari, who served as the technical monitor, for his support, cooperation and understanding during the performance of the contract. We acknowledge the NAS computer resources supplied by NASA. Special thanks are due to Dr. James M. Luckring, Head, Transonic/Supersonic Aerodynamics Branch, for giving us the opportunity to participate in this project.

Aerodynamics Department

Lockheed Aeronautical Systems Company

Marietta, Georgia 30063

October 24, 1994

REFERENCES

1. Raj, P., Olling, C.R., Sikora, J.S., Keen, J.M., Singer, S.W. and Brennan, J.E., "Three-dimensional Euler/Navier-Stokes Aerodynamic Method (TEAM), Vol. I: Computational Method and Verification," WRDC-TR-87-3074 (Revised), June 1989.

2. Goble, B.D., Raj, P., and Kinard, T.A., "Three-dimensional Euler/Navier-Stokes Aerodynamic Method (TEAM) Upgrade, Version 713 User's Manual," WL-TR-93-3115, Feb. 1994.

3. Buning, P.G., Chan, W.M., Renze, K.J., Sondak, D.L., Chiu, I.T., and Slotnick, J.P., "OVERFLOW User's Manual, Version 1.6ap," NASA-Ames Research Center, Moffett Field, California, March 1994.

4. Howlett, D. and Finley, D., personal communication, Lockheed Fort Worth Company.

5. Frink, N.T., Parikh, P., and Pirzadeh, S., "A Fast Upwind Solver for the Euler Equations on Three-dimensional Unstructured Meshes," AIAA 91-0102, January 1991.

6. Raj, P., Sikora, J.S., and Keen, J.M., "Free-Vortex Flow Simulation Using a Three-dimensional Euler Aerodynamic Method," *Journal of Aircraft*, Vol. 25, No. 2, Feb. 1988, pp. 128-134.

7. Raj, P., Keen, J.M., and Singer, S.W., "Applications of an Euler Aerodynamic Method to Free-Vortex Flow Simulation," *Journal of Aircraft*, Vol. 27, No. 11, Nov. 1990, pp. 941-949.

8. Raj, P., "Aerodynamic Analysis Using Euler Equations: Capabilities and Limitations," Chapter 18, *Applied Computational Aerodynamics*, Progress in Astronautics and Aeronautics, Volume 125, AIAA, Washington, DC, 1990, P.A. Henne (ed.).

9. Ghaffari, F., Luckring, J.M., Thomas, J.L., and Bates, B.L., "Navier-Stokes Solutions about the F/A-18 Forebody-LEX Configuration," AIAA Paper 89-0338, Jan. 1989.

10. Olling, C.R. and Mani, K.K., "Navier-Stokes and Euler Computations of the Flow Field around a Complete Aircraft," *Advanced Aerospace Aerodynamics*, SAE SP-757, Oct. 1988, pp. 231-242.

11. Flores, J. and Chaderjian, N.M., "The Numerical Simulation of Transonic Separated Flow About the Complete F-16A," AIAA Paper 88-2506, June 1988.

12. Ghaffari, F., personal communication, NASA Langley Research Center, 1994.

13. Steinbrenner, J.P. and Chawner, J.R., "The GRIDGEN Version 8 Multiple Block Grid Generation Software," MDA Engineering Report 92-01, December 1992.

14. Walatka, P.P., Clucas, J., McCabe, K., Plessel, T. and Potter, R., "FAST User Guide," RND-92-015, NASA-Ames Research Center, Moffett Field, California, November 1992.

15. Turner, P.J., "ACE/gr User's Manual," Center for Coastal and Land-Margin Research, Oregon Graduate Institute of Science and Technology, Beaverton, Oregon, 97006-1999, 1993

16. Raj, P. and Harris, B.W.,"Using Surface Transpiration with an Euler Method for Cost-effective Aerodynamic Analysis," AIAA 93-3506, August 1993.

17. Thomas, J.L., Taylor, S.L., and Anderson, W.L., "Navier-Stokes Computations of Vortical Flows Over Low Aspect Ratio Wings," AIAA Paper 87-0207, 1987.

18. Strang, W.Z., "QBERT: A Grid Evaluation Code," AFWAL-TM-88-193, July 1988.

19. Baldwin, B.S. and Lomax, H., "Thin Layer Approximation and Algebraic Model for Separated Turbulent Flows," AIAA 78-257, January 1978.

20. Degani, D. and Schiff, L.B., "Computation of Supersonic Viscous Flows Around Pointed Bodies at Large Incidence, AIAA 83-0034, January 1983.

Benign vortex flow, M = 0.4, α = 10.1°			
	C_L	C_D	C_m
TEAM Euler Inviscid	0.529	0.1024*	-0.0581
TEAM RANS Viscous	0.473	0.0836	-0.0363
Test	0.542	0.0929	-0.0512

*includes C_{Do} of 0.02

Table 1. MTVI twin-tail baseline model force and moment data correlation for benign vortex flow

Benign vortex flow, M = 0.4, α = 10.1°			
	C_L	C_D	C_m
TEAM Euler Coarse	0.517	0.1007*	-0.0549
TEAM Euler Fine	0.529	0.1024*	-0.0581
Test	0.542	0.0929	-0.0512

*includes C_{Do} of 0.02

Table 2. Euler solution grid sensitivity, MTVI twin-tail baseline model, benign vortex flow

Burst vortex flow, M = 0.4, α = 35.21°			
	C_L	C_D	C_m
TEAM Euler Inviscid	1.33	0.91*	0.1
TEAM RANS Viscous	1.23	0.83	0.17
Test	1.234	0.846	0.0657

*includes C_{Do} of 0.02

Table 3. MTVI twin-tail baseline model force and moment data correlation for burst vortex flow

Benign vortex flow, M = 0.4, α = 10.1°			
	C_L	C_D	C_m
TEAM Euler Inviscid	0.5739	0.114*	–0.0865
TEAM RANS Viscous	0.492	0.087	–0.0462
Test	0.518	0.0928	–0.0462

*includes C_{Do} of 0.02

Table 4. MTVI single-tail baseline model force and moment data correlation for benign vortex flow

Burst vortex flow, M = 0.4, α = 35.35°			
	C_L	C_D	C_m
TEAM Euler Inviscid	1.7	1.14*	0.12
TEAM RANS Viscous	1.4	0.9	0.1
Test	1.416	0.98	0.0187

*includes C_{Do} of 0.02

Table 5. MTVI single-tail baseline model force and moment data correlation for burst vortex flow

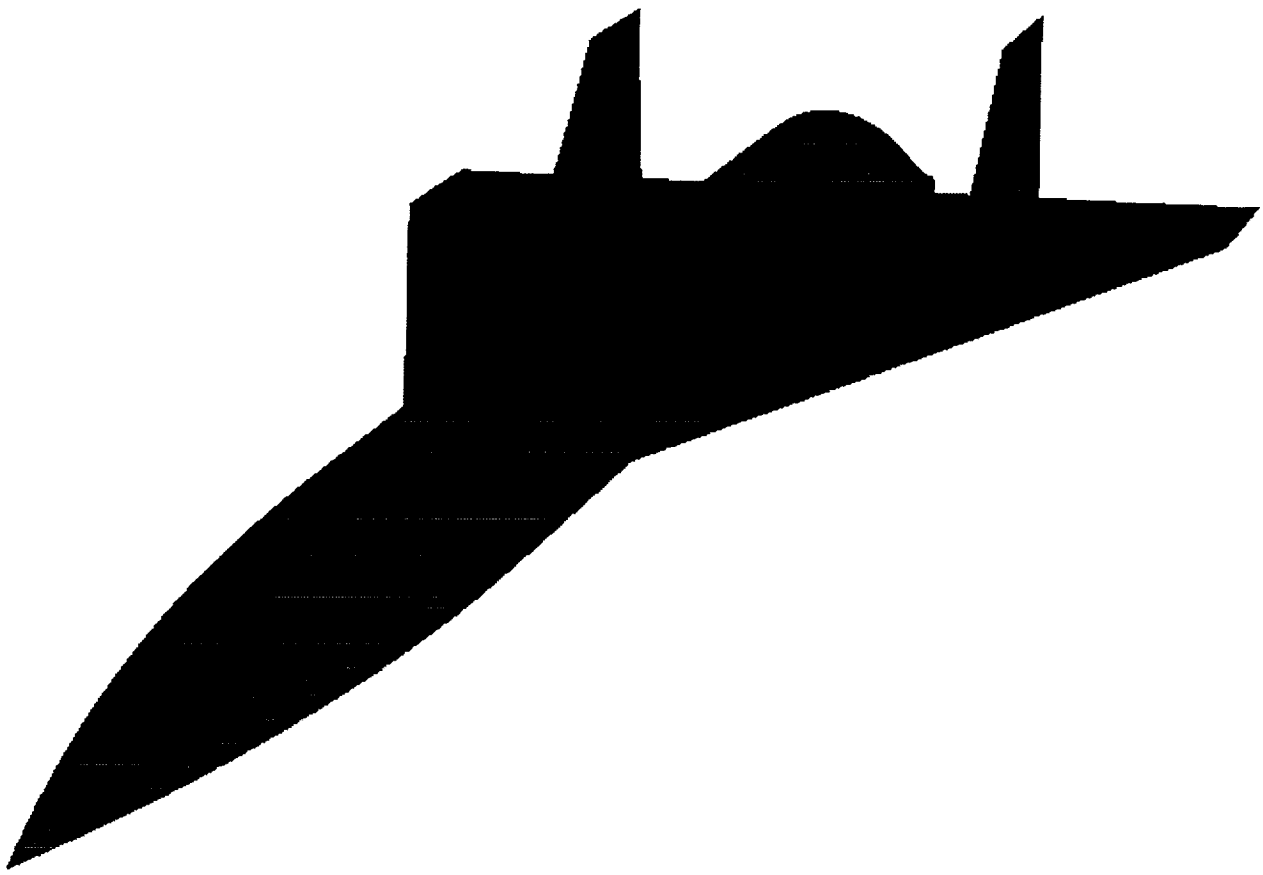

Geometric parameters (Full configuration; all dimensions in inches)

Area (S_{ref})	208.224
Chord (c)	10.92
Span (b)	19.2
Moment Center (from nose)	(20.335, 0, 0)
Chine angle (included)	100°
Wing leading-edge sweep	60°

Figure 1. Geometry of MTVI twin-tail baseline model

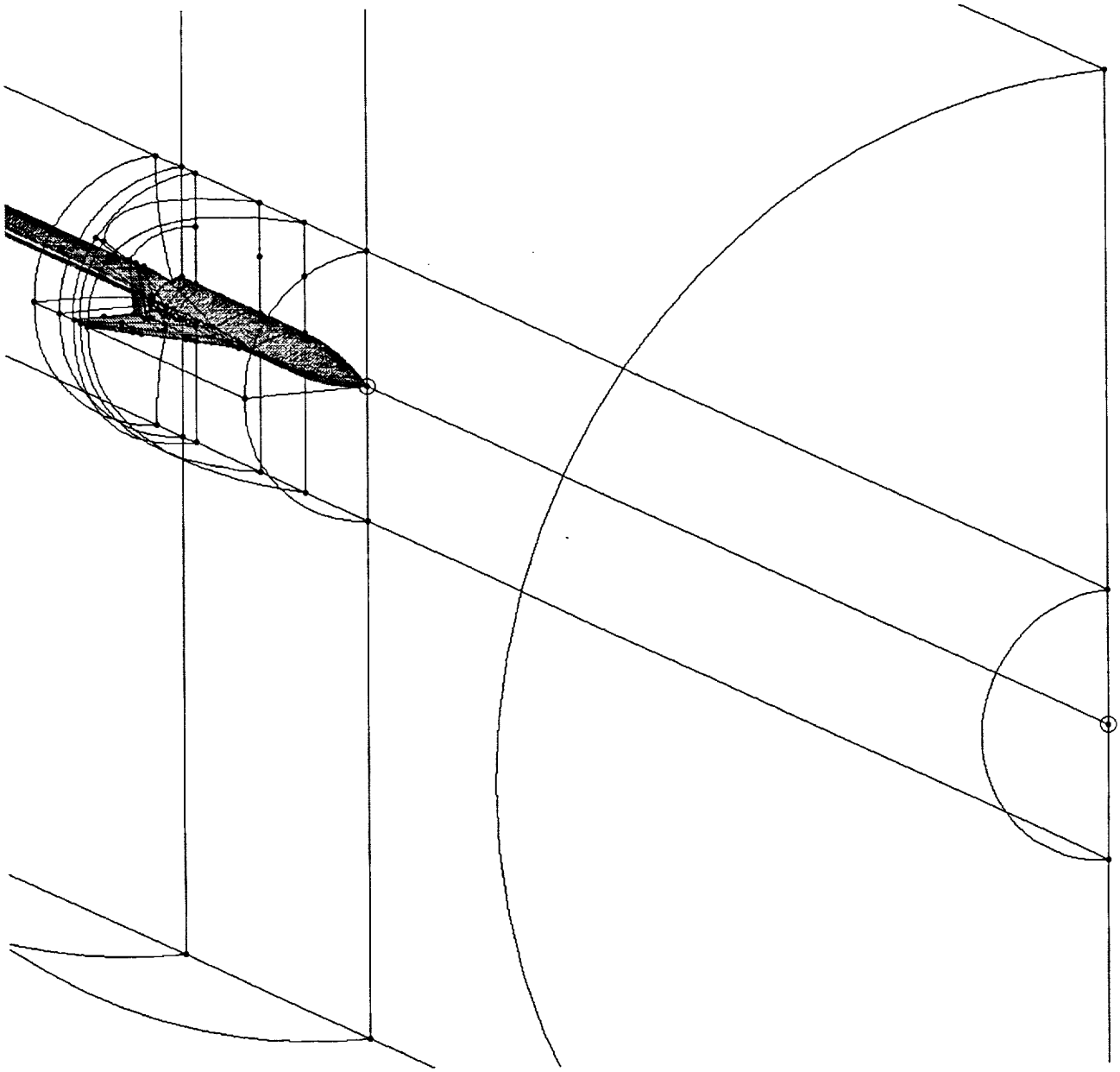

16 Zones

Topology O-H

Euler:

Fine:	1,866,224 nodes
Coarse:	1,119,605 nodes
Viscous:	2,196,294 nodes

Far Field Locations:

Upstream:	4 Body Lengths
Downstream:	5 Body Lengths
Radial:	5 Span Lengths

Grid Generation Time:

Euler:	64 labor-hours	Viscous:	40 additional labor-hours

Figure 2. Grid blocks Schematic and grid generation data for twin-tail model

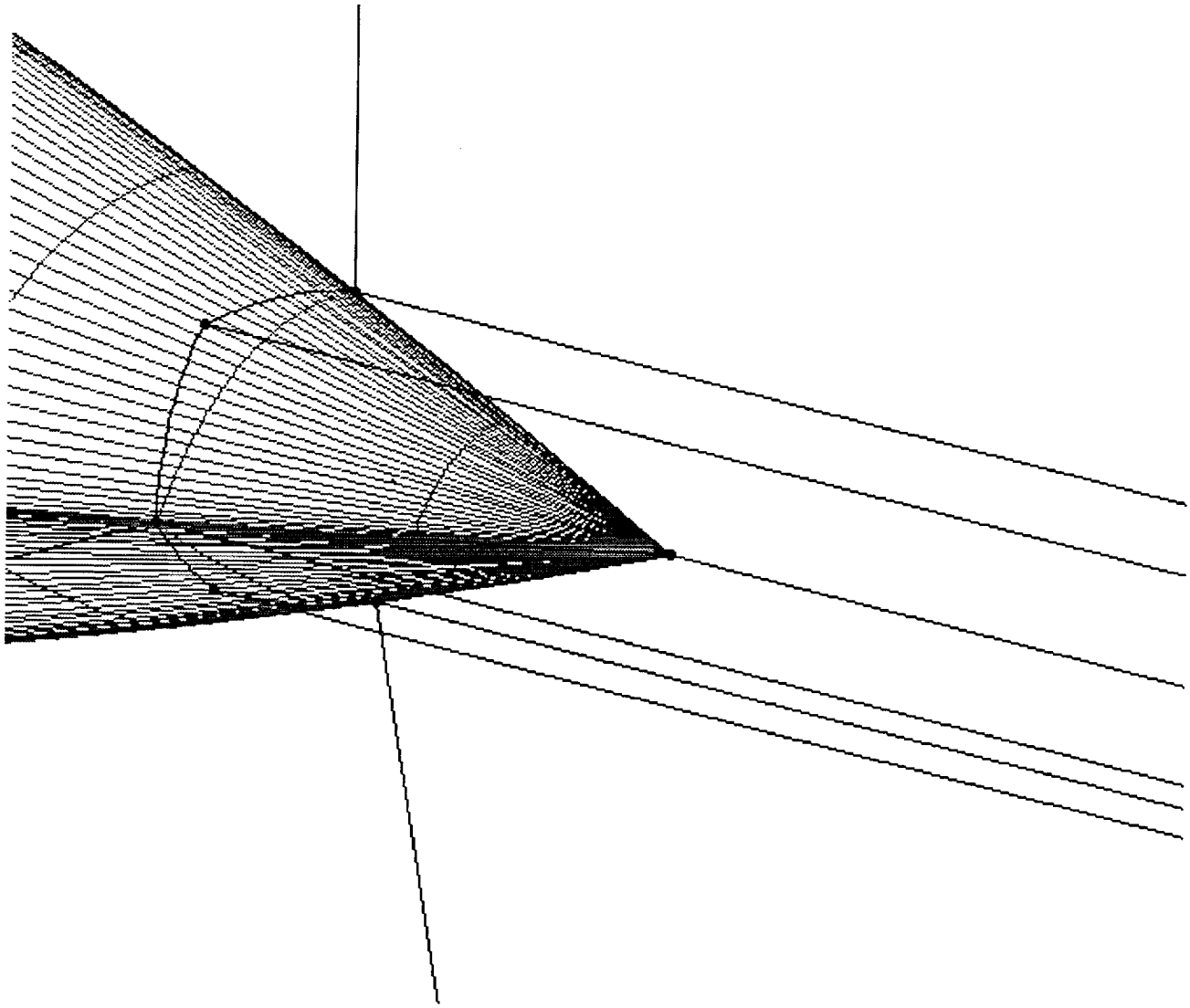

Figure 3. Schematic of blocks used to eliminate pole boundary

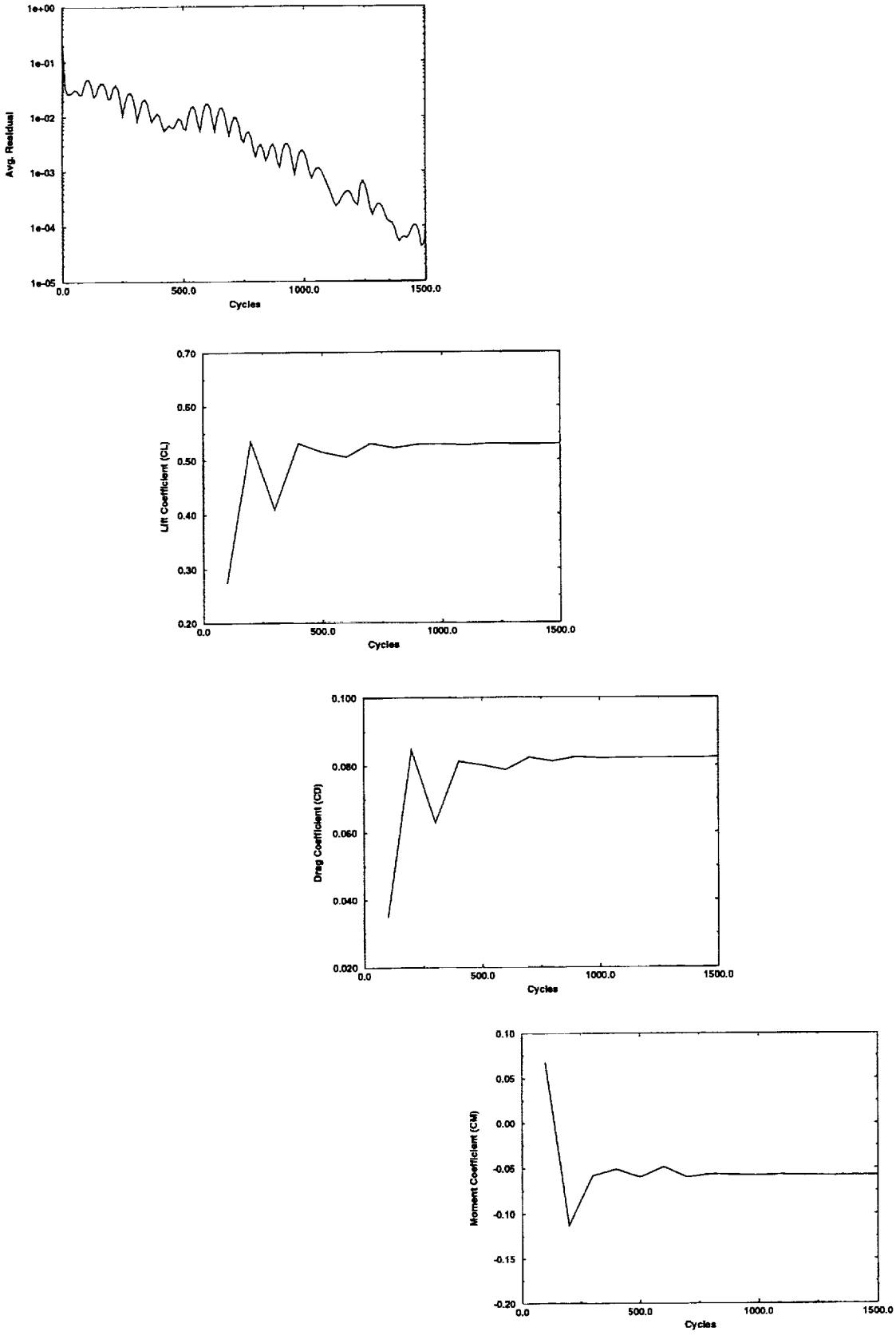

Figure 4. Average residual, lift, drag, and moment convergence histories for TEAM Euler analysis of twin-tail model, M = 0.4, $\alpha = 10.1^{0}$

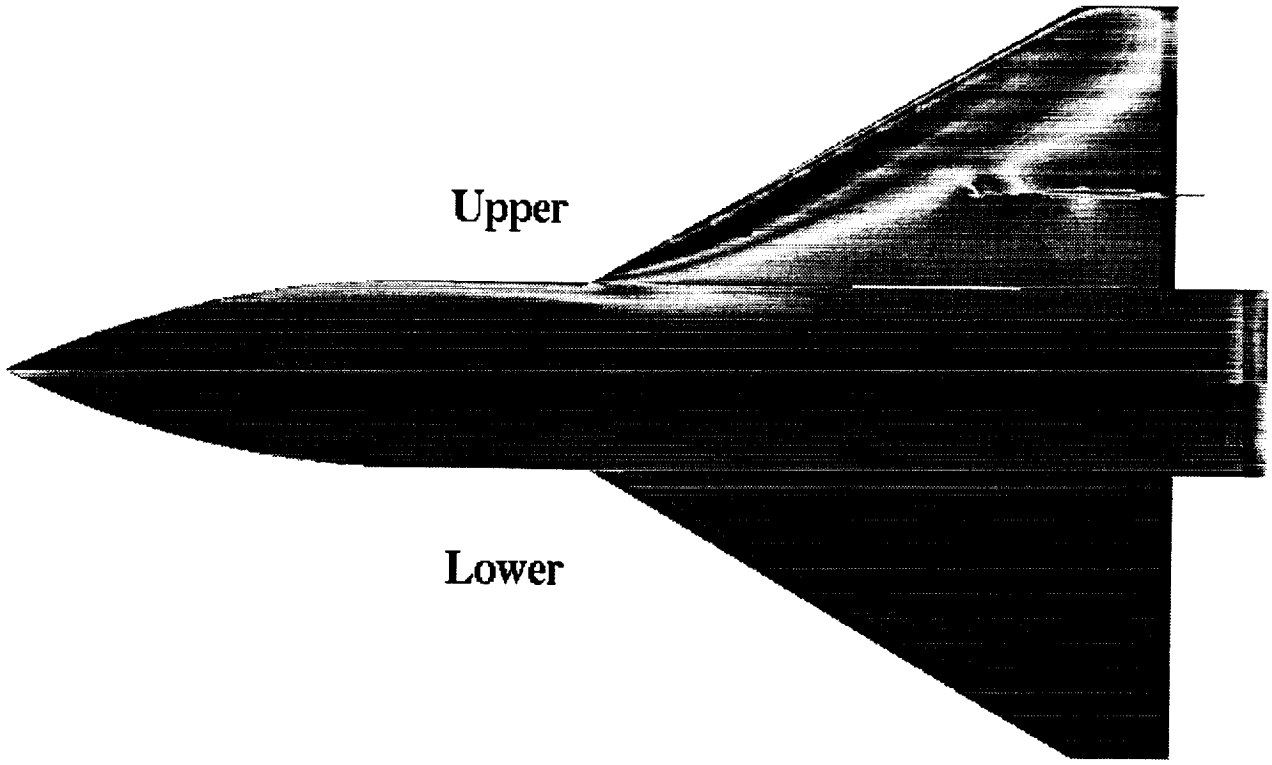

Figure 5. Surface C_p distribution, TEAM Euler solution of benign vortex flow, twin-tail model M = 0.4, $\alpha = 10.1^o$

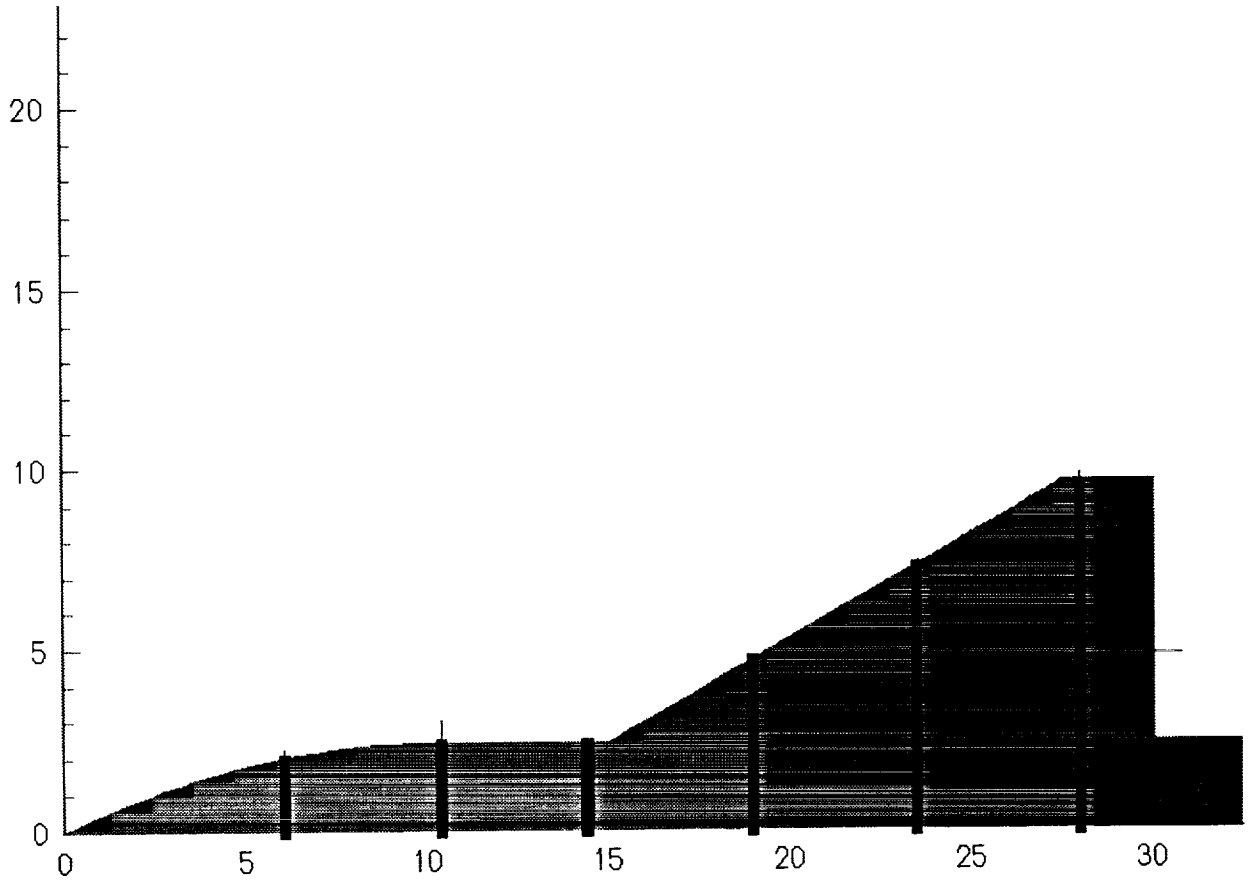

Forebody Stations:	Aft-fuselage and Wing Stations:
x = 6.11	x = 19.05
x = 10.45	x = 23.55
x = 14.5	x = 28.05

Figure 6. Test data cross-flow stations

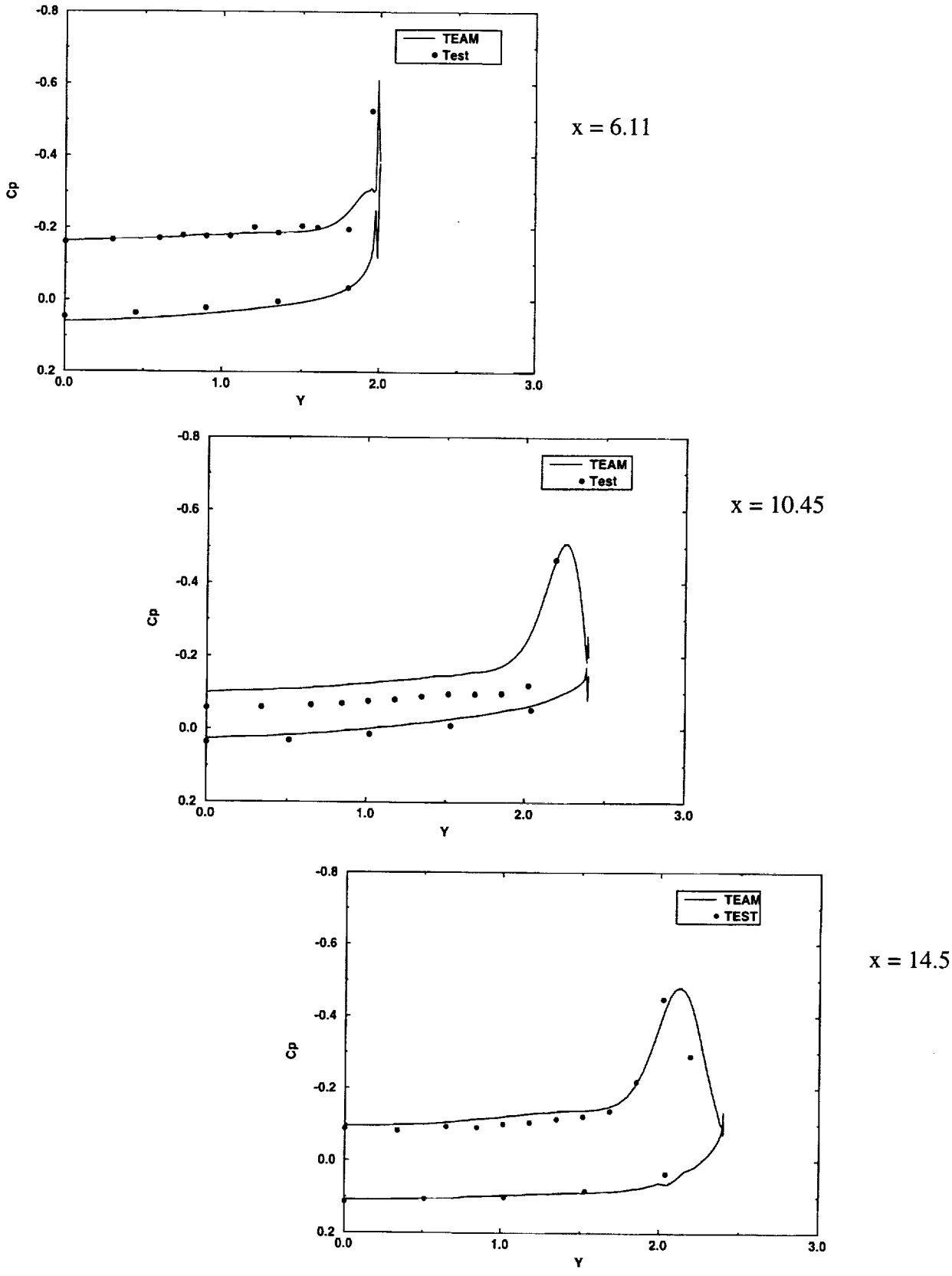

Figure 7. Surface C_p comparisons of TEAM Euler solutions with test data at three forebody stations, benign vortex flow, twin-tail model, M = 0.4, $\alpha = 10.1^{\circ}$

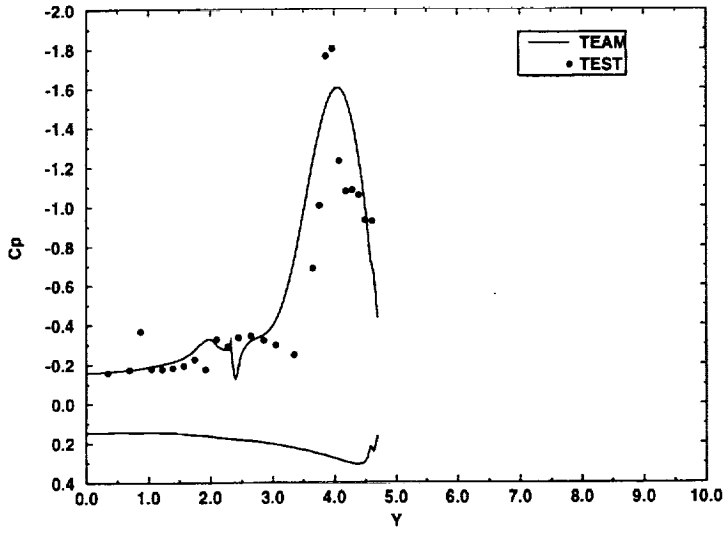

x = 19.05

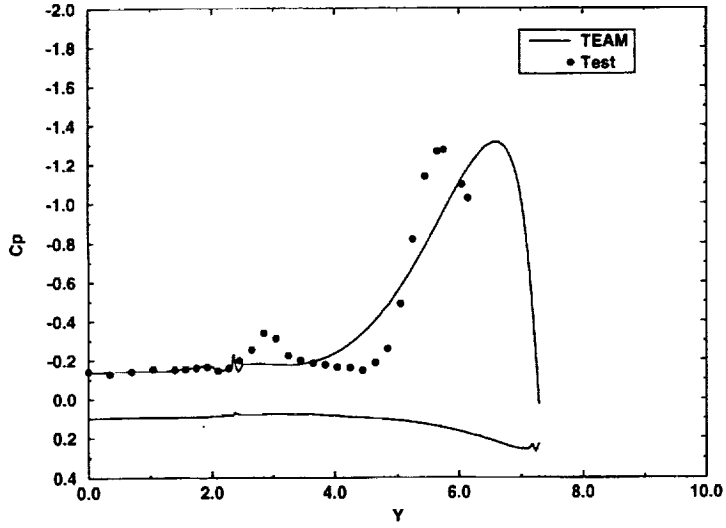

x = 23.55

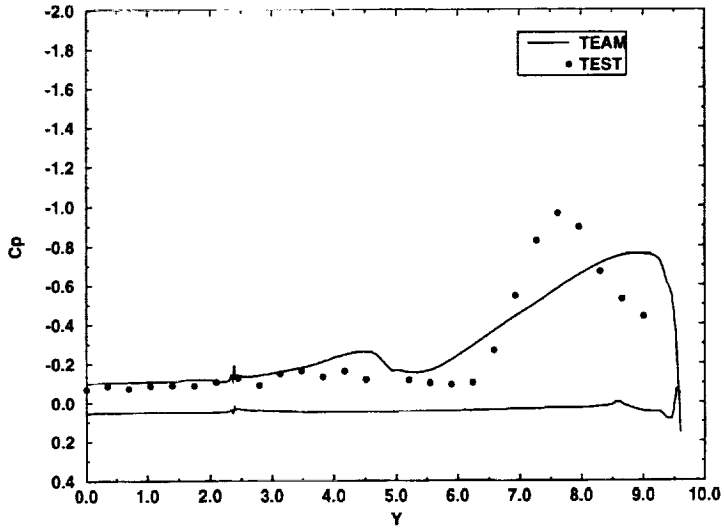

x = 28.05

Figure 8. Surface C_p comparisons of TEAM Euler solutions with test data at three aft-fuselage and wing stations, benign vortex flow, twin-tail model, M = 0.4, $\alpha = 10.1^o$

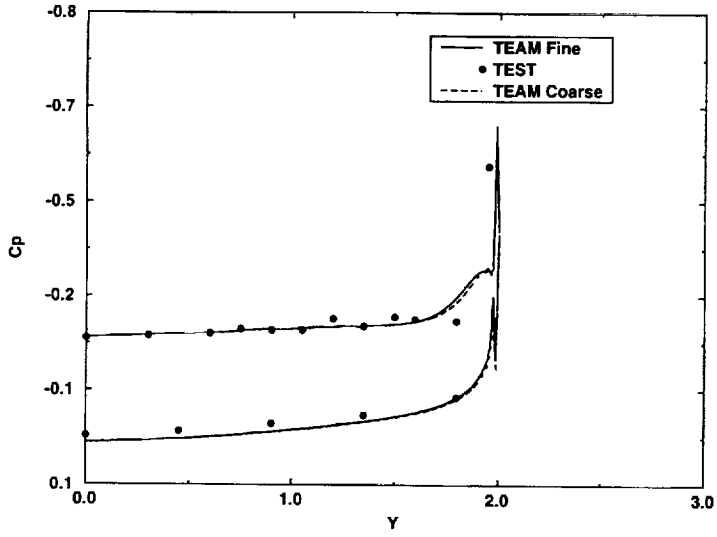

x = 6.11

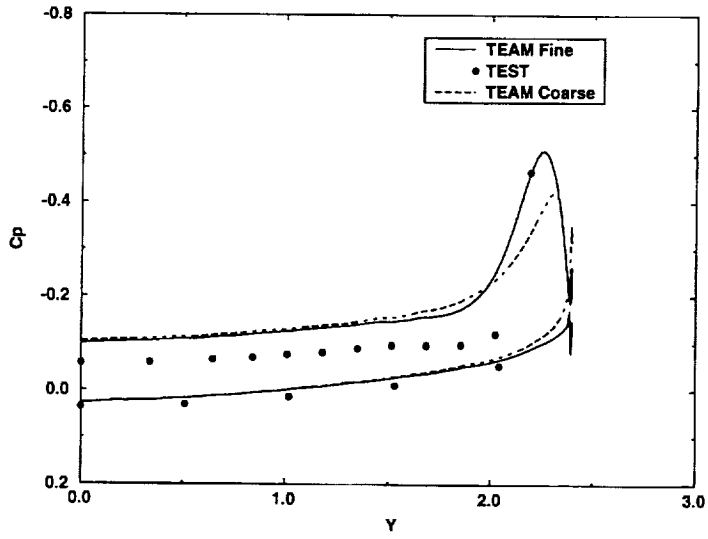

x = 10.45

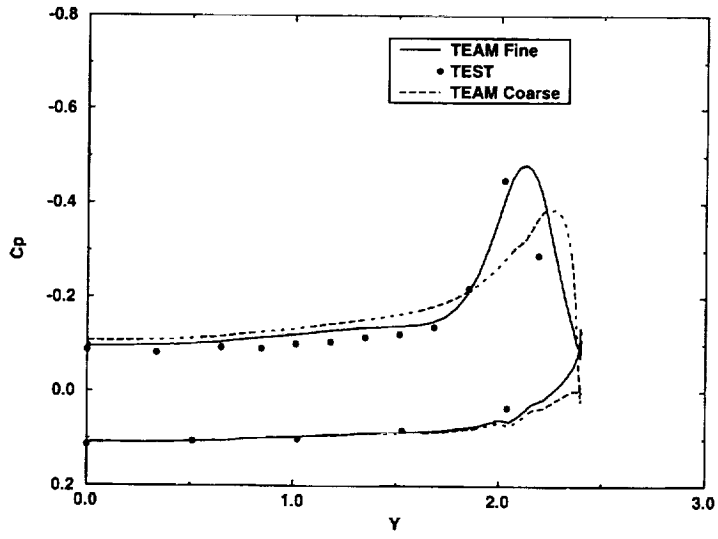

x = 14.5

Figure 9. Grid sensitivity of surface C_p on the three forebody stations for TEAM Euler solution of benign vortex flow, twin-tail model, M = 0.4, $\alpha = 10.1^o$

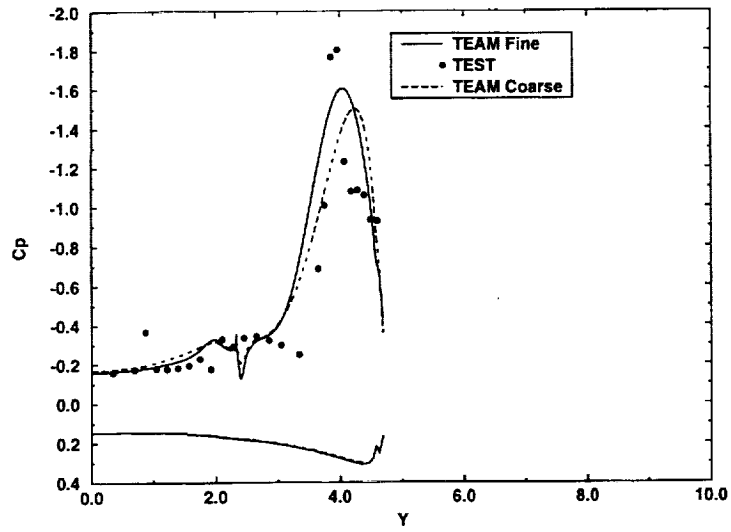

x = 19.05

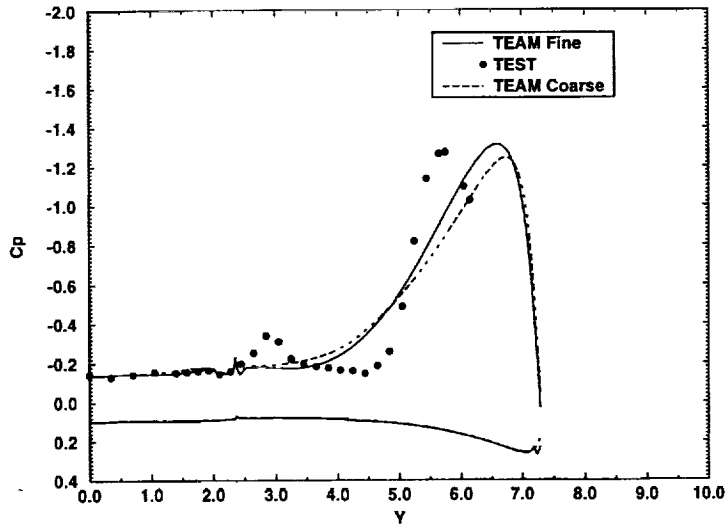

x = 23.55

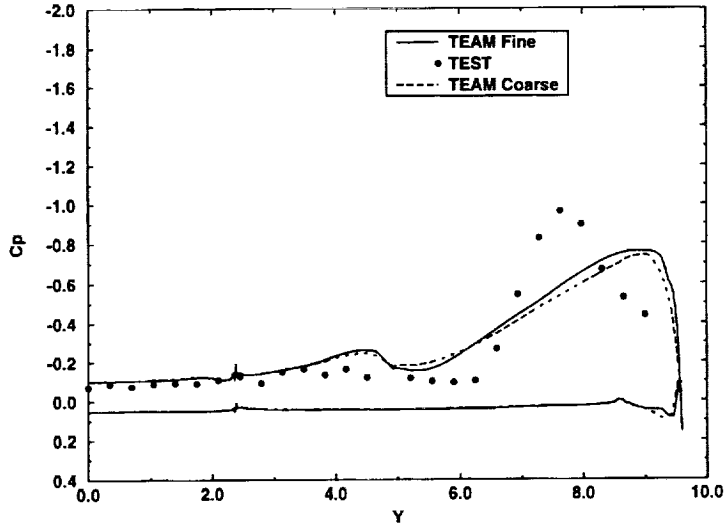

x = 28.05

Figure 10. Grid sensitivity of surface C_p on the three aft-fuselage and wing stations for TEAM Euler solution of benign vortex flow, twin-tail model, M = 0.4, $\alpha = 10.1^o$

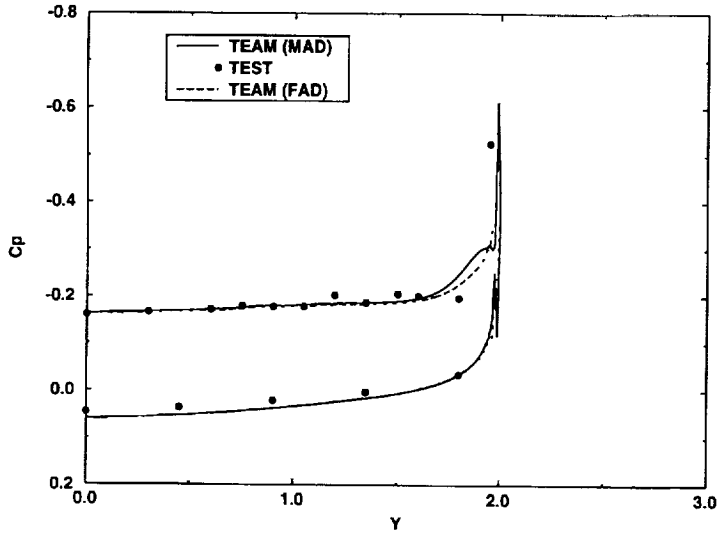

x = 6.11

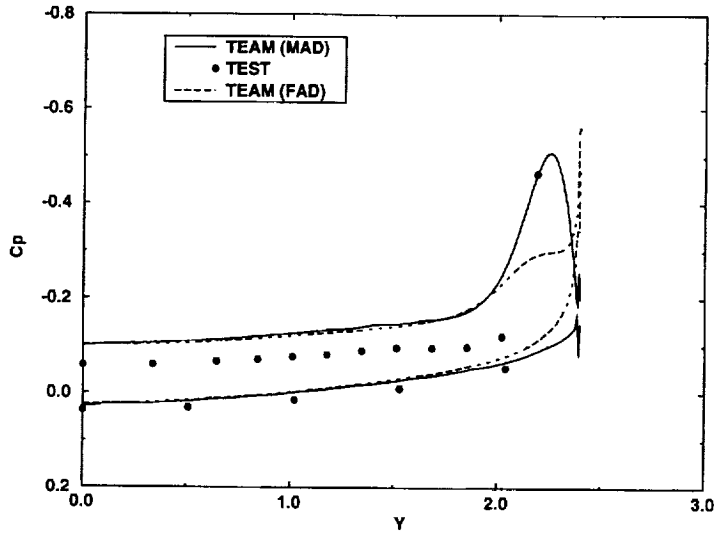

x = 10.45

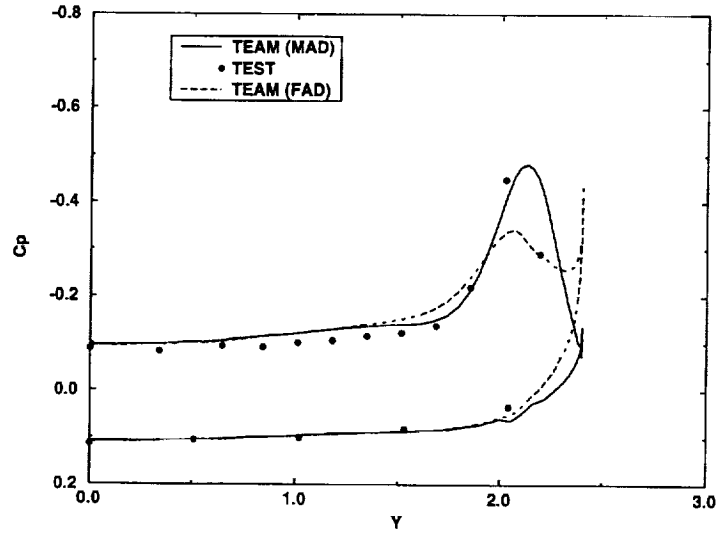

x = 14.5

Figure 11. Numerical dissipation effect on surface C_p at the three forebody stations for TEAM Euler solution of benign vortex flow, twin-tail model, M = 0.4, $\alpha = 10.1^{\circ}$

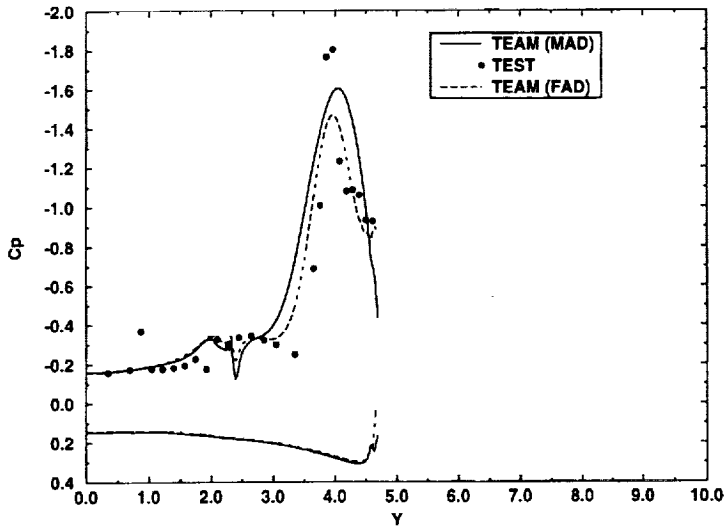

x = 19.05

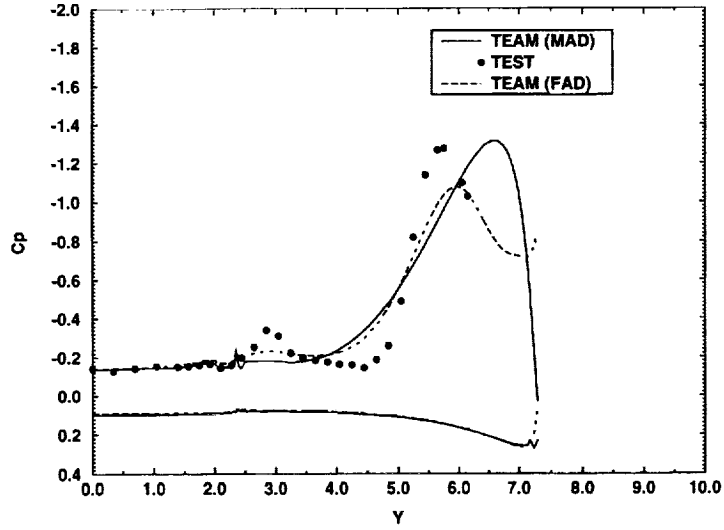

x = 23.55

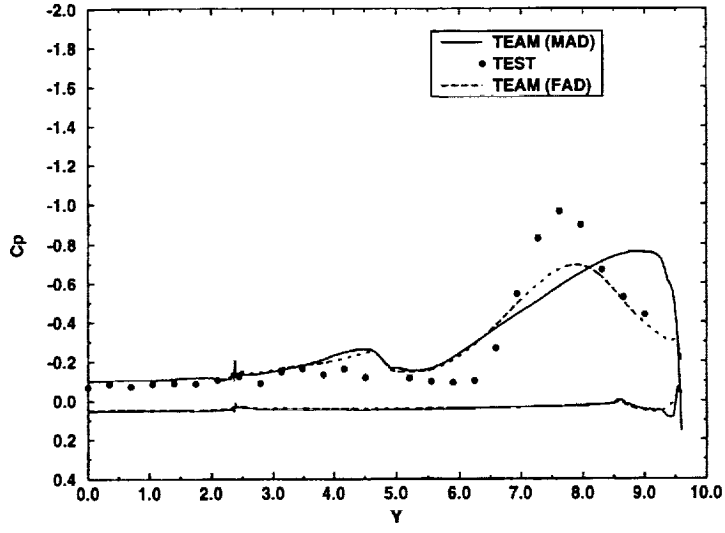

x = 28.05

Figure 12. Numerical dissipation effect on surface C_p at the three aft-fuselage and wing stations for TEAM Euler solution of benign vortex flow, twin-tail model, M = 0.4, $\alpha = 10.1^o$

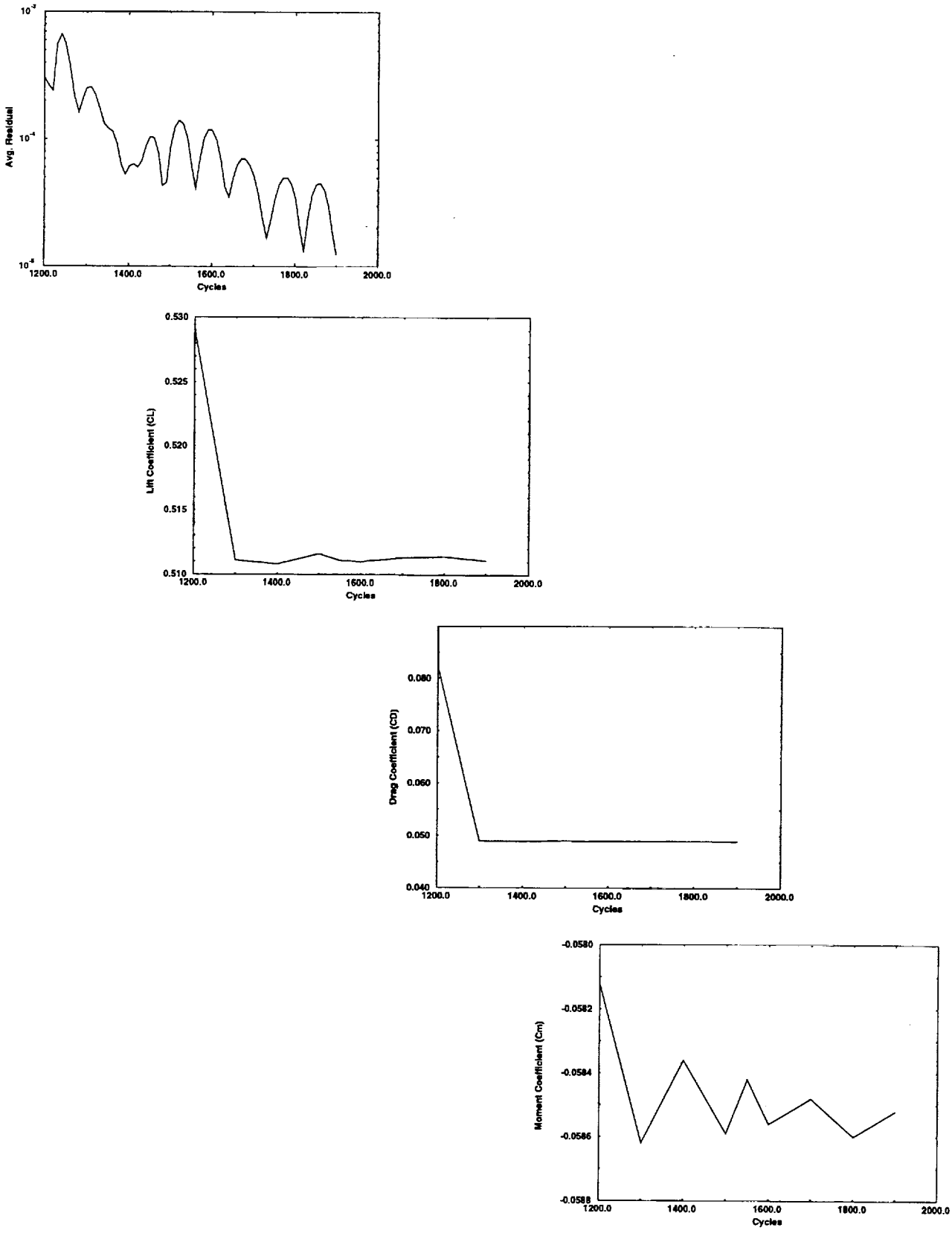

Figure 13. Average residual, lift, drag, and moment convergence histories for simulated leading-edge flap deflection 30° down, twin-tail model, TEAM Euler solution, M = 0.4 α = 10.1°

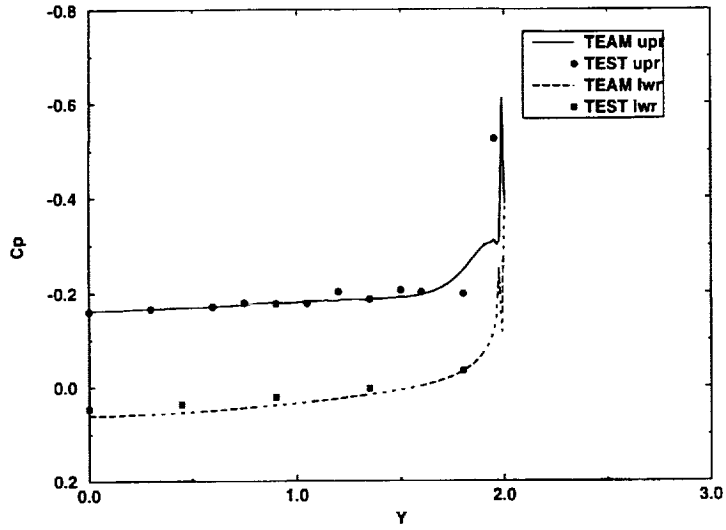

x = 6.11

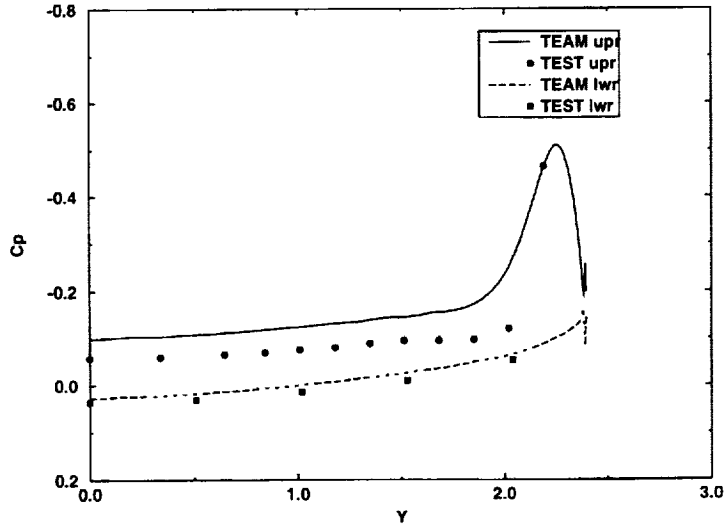

x = 10.45

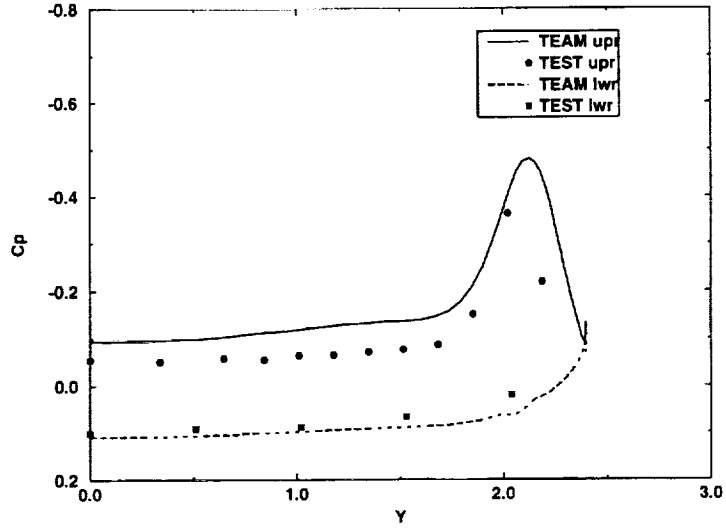

x = 14.5

Figure 14. Surface C_p distributions at three forebody stations for simulated leading-edge flap deflection 30° down, twin-tail model, TEAM Euler solution, M = 0.4, α = 10.1°

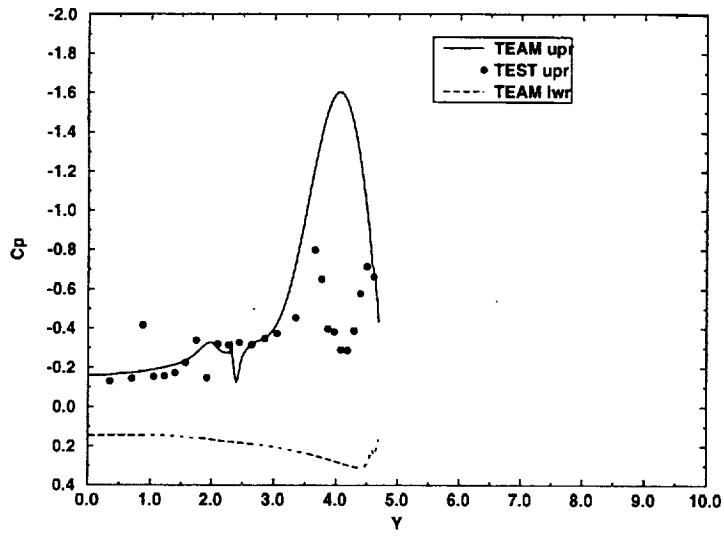

x = 19.05

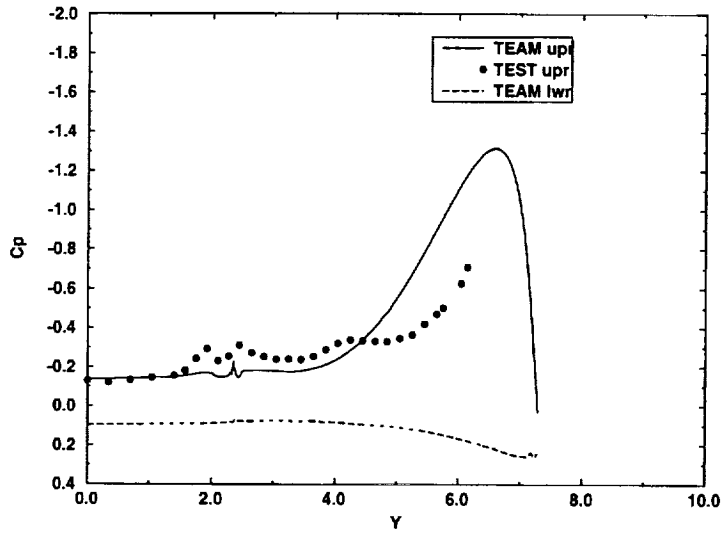

x = 23.55

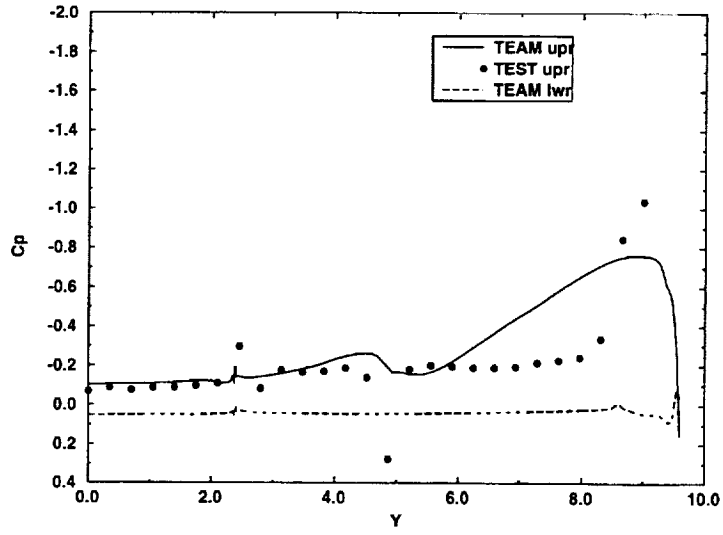

x = 28.05

Figure 15. Surface Cp distributions at three aft-fuselage and wing stations for simulated leading-edge flap deflection 30° down, twin-tail model, TEAM Euler solution, M = 0.4, $\alpha = 10.1^{\circ}$

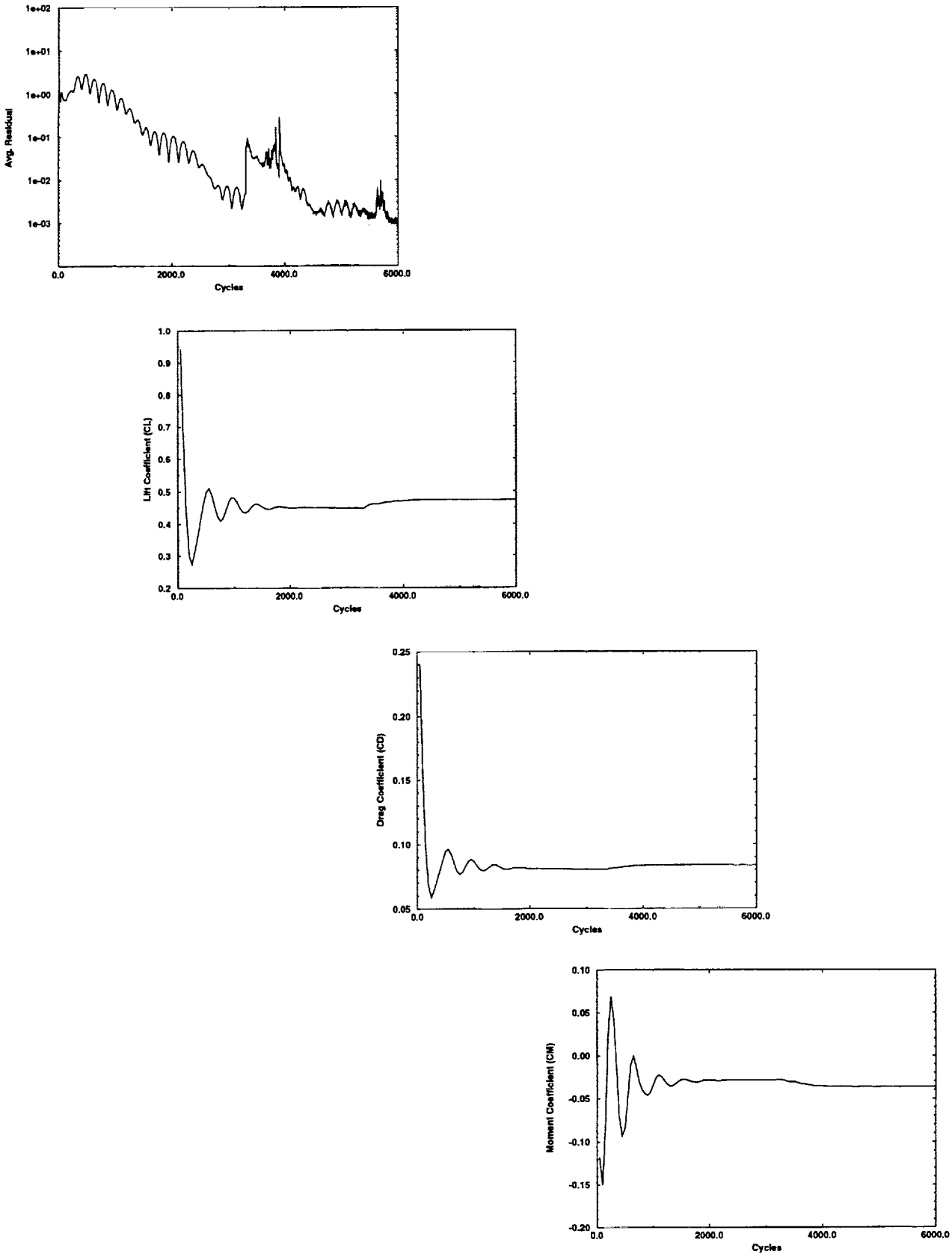

Figure 16. Average residual, lift, drag, and moment convergence histories, twin-tail model, TEAM RANS viscous solution, M = 0.4, $\alpha = 10.1^{o}$, Re = 2.7 million

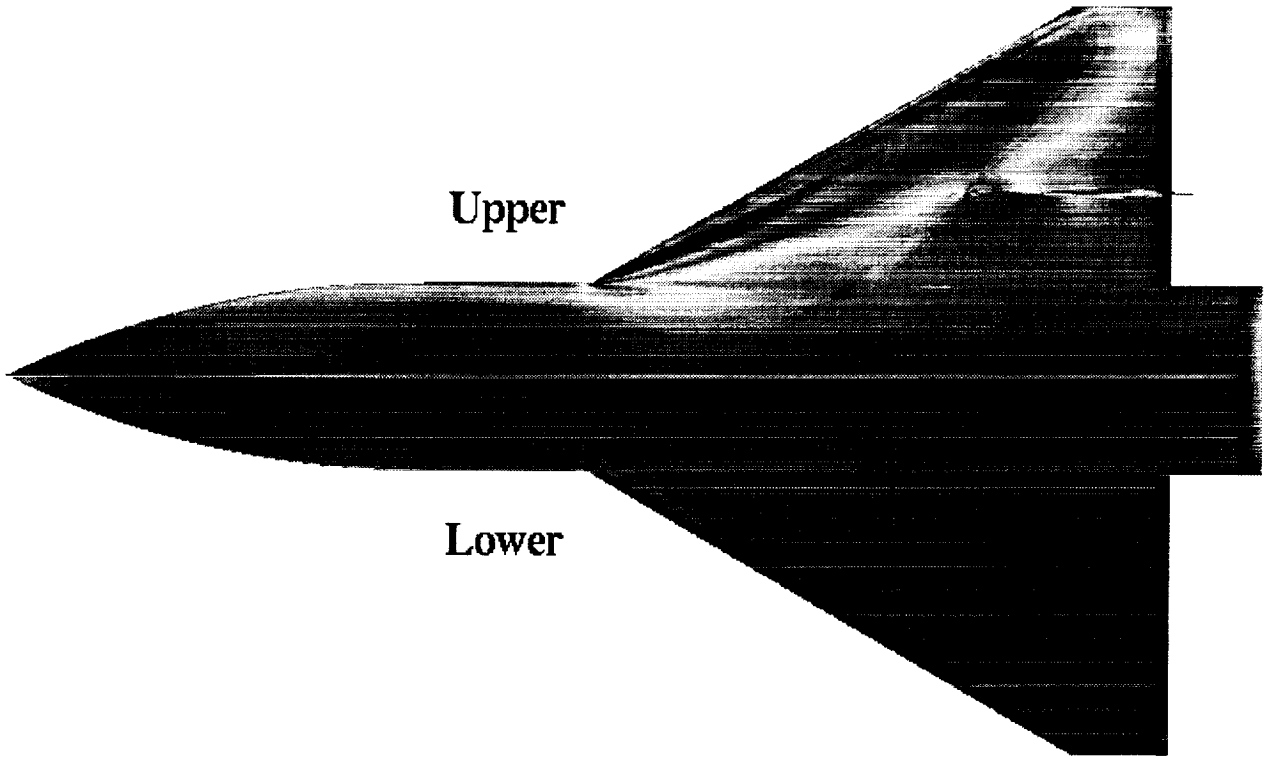

Figure 17. Surface Cp distribution, TEAM RANS viscous solution, twin-tail model, M = 0.4, $\alpha = 10.1^{o}$, Re = 2.7 million

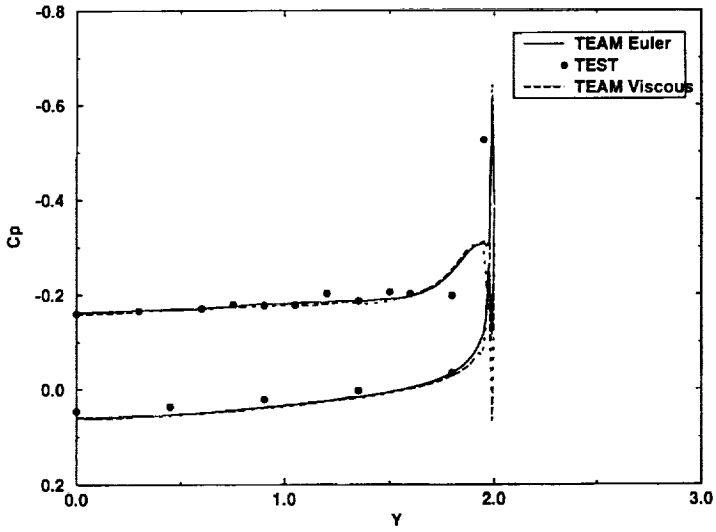

x = 6.11

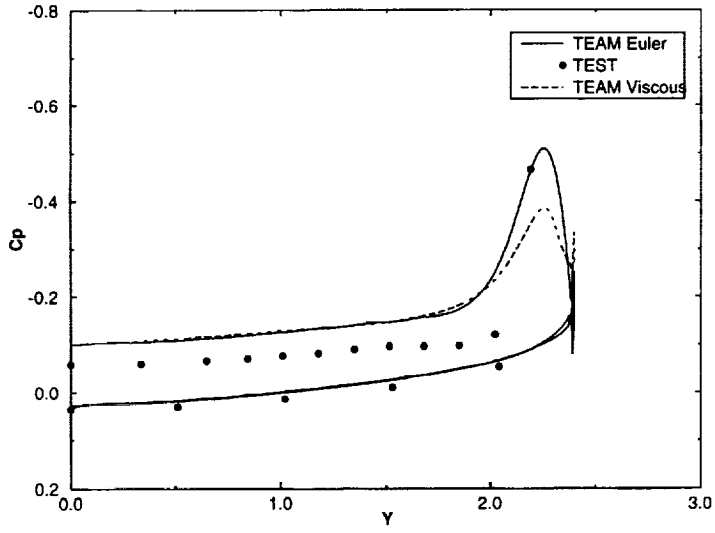

x = 10.45

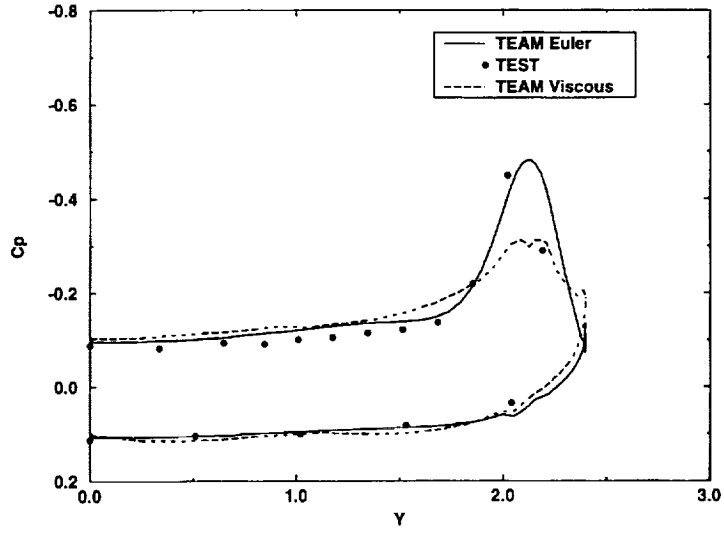

x = 14.5

Figure 18. Viscous effects on surface pressures at the three forebody stations for benign vortex flow, twin-tail model, M = 0.4, $\alpha = 10.1^{\circ}$, Re = 2.7 million

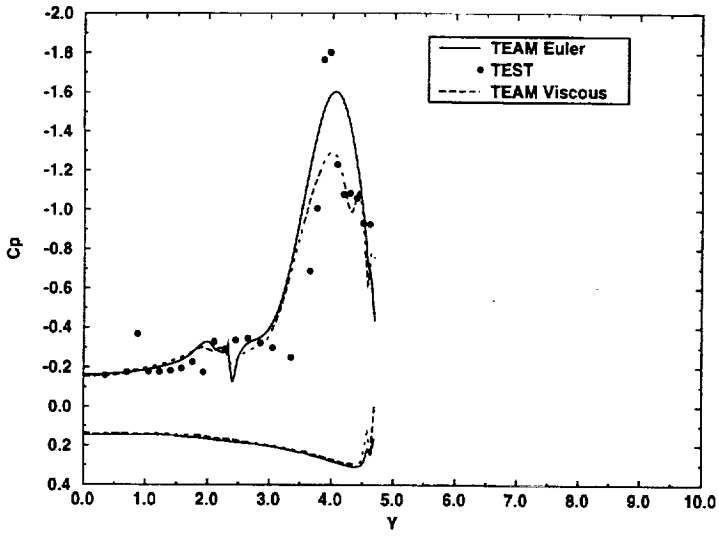

x = 19.05

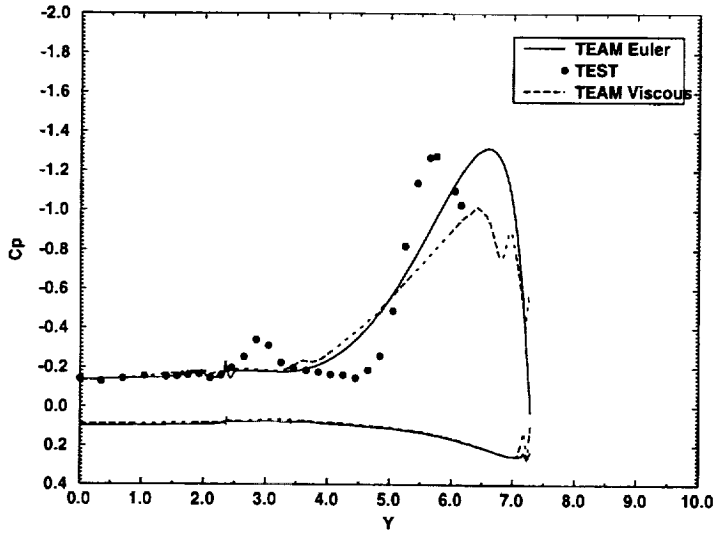

x = 23.55

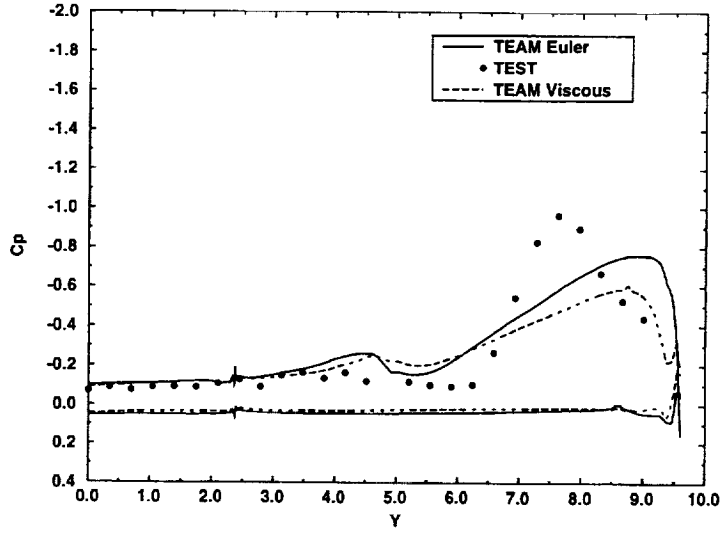

x = 28.05

Figure 19. Viscous effects on surface pressures at the three aft-fuselage and wing stations for benign vortex flow, twin-tail model, M = 0.4, $\alpha = 10.1^{\circ}$, Re = 2.7 million

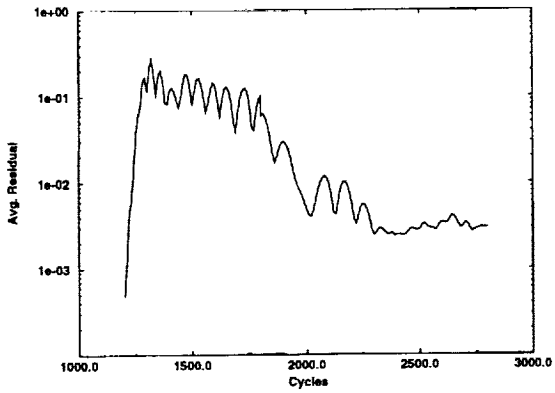

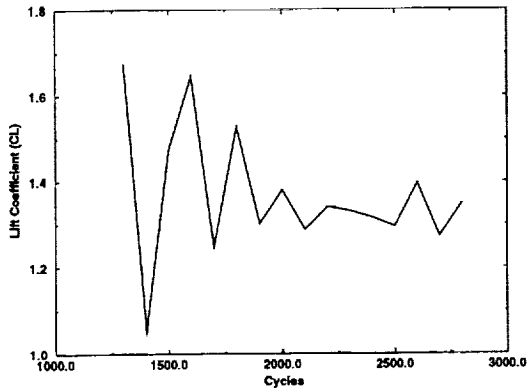

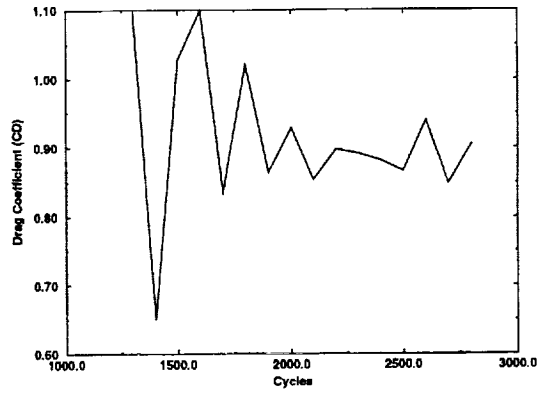

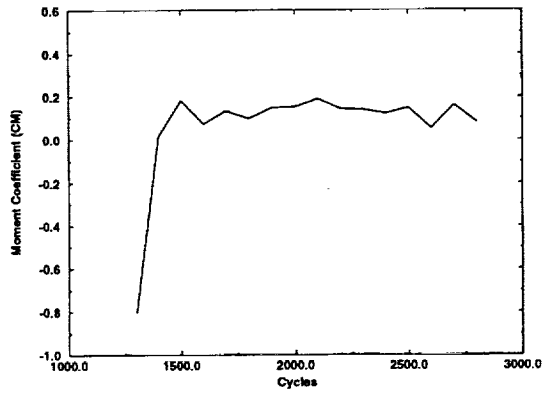

Figure 20. Average residual, lift, drag, and moment convergence histories for TEAM Euler analysis, twin-tail model, M = 0.4, $\alpha = 35.21^{0}$

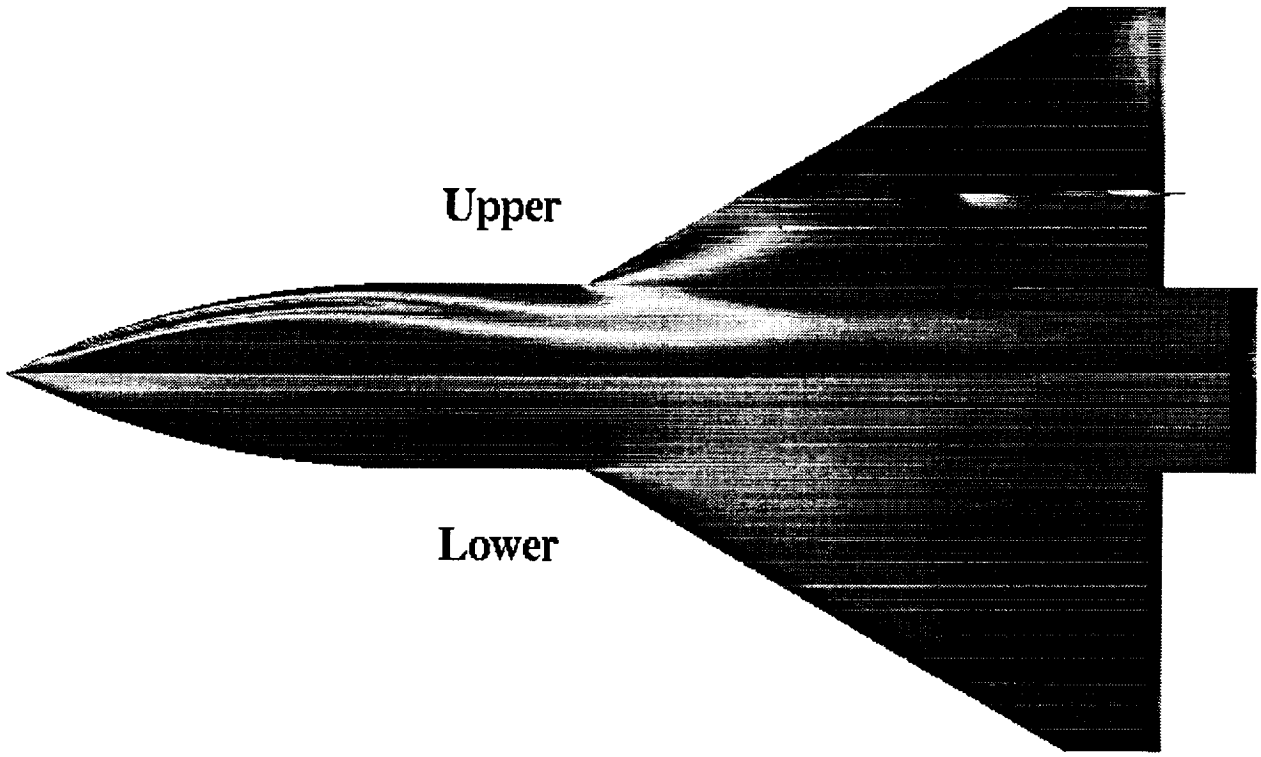

Figure 21. Surface Cp distribution, TEAM Euler solution of burst vortex flow, twin-tail model, M = 0.4, $\alpha = 35.21^{o}$

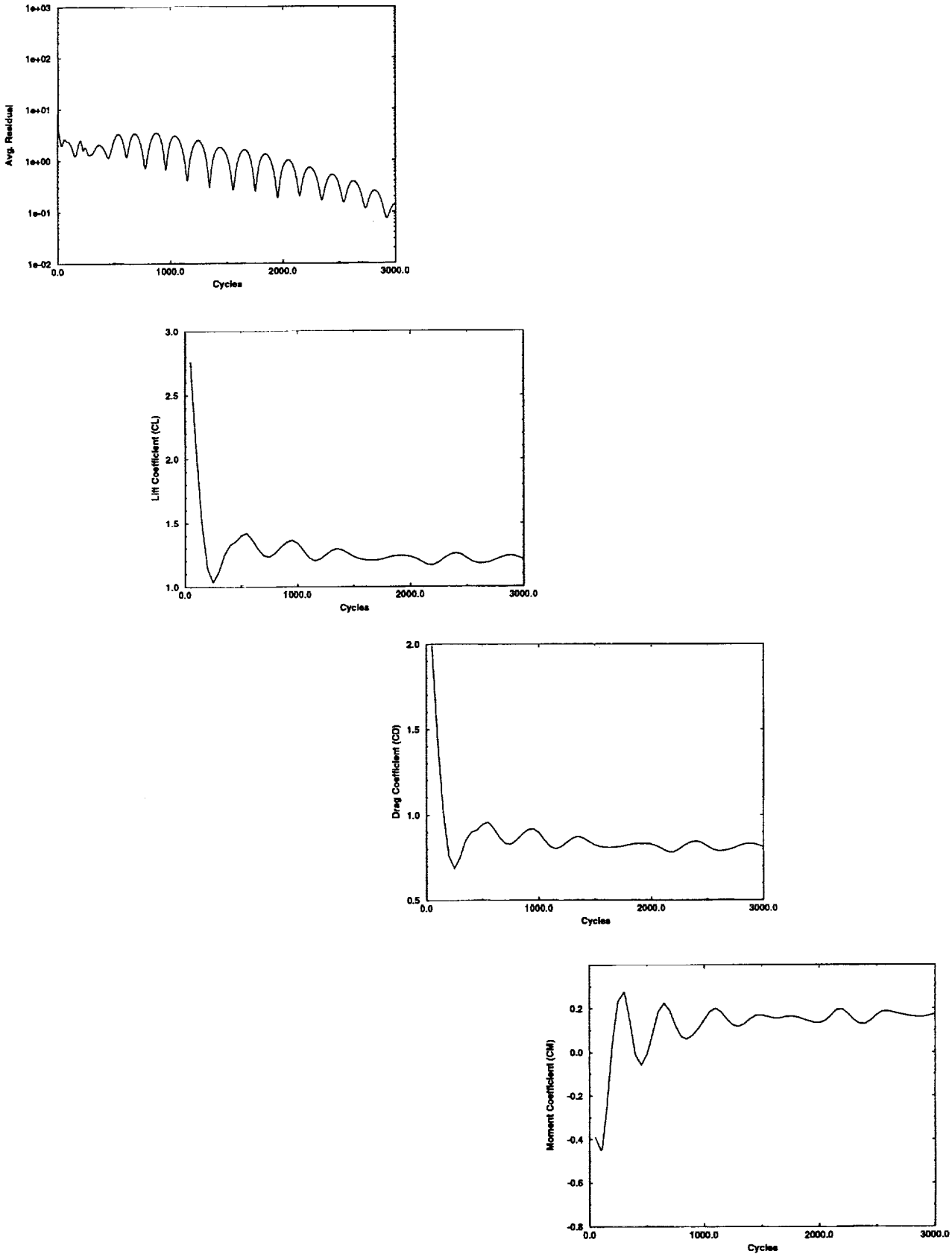

Figure 22. Average residual, lift, drag, and moment convergence histories for TEAM RANS viscous analysis, twin-tail model, M = 0.4, $\alpha = 35.21^{o}$, Re = 2.7 million

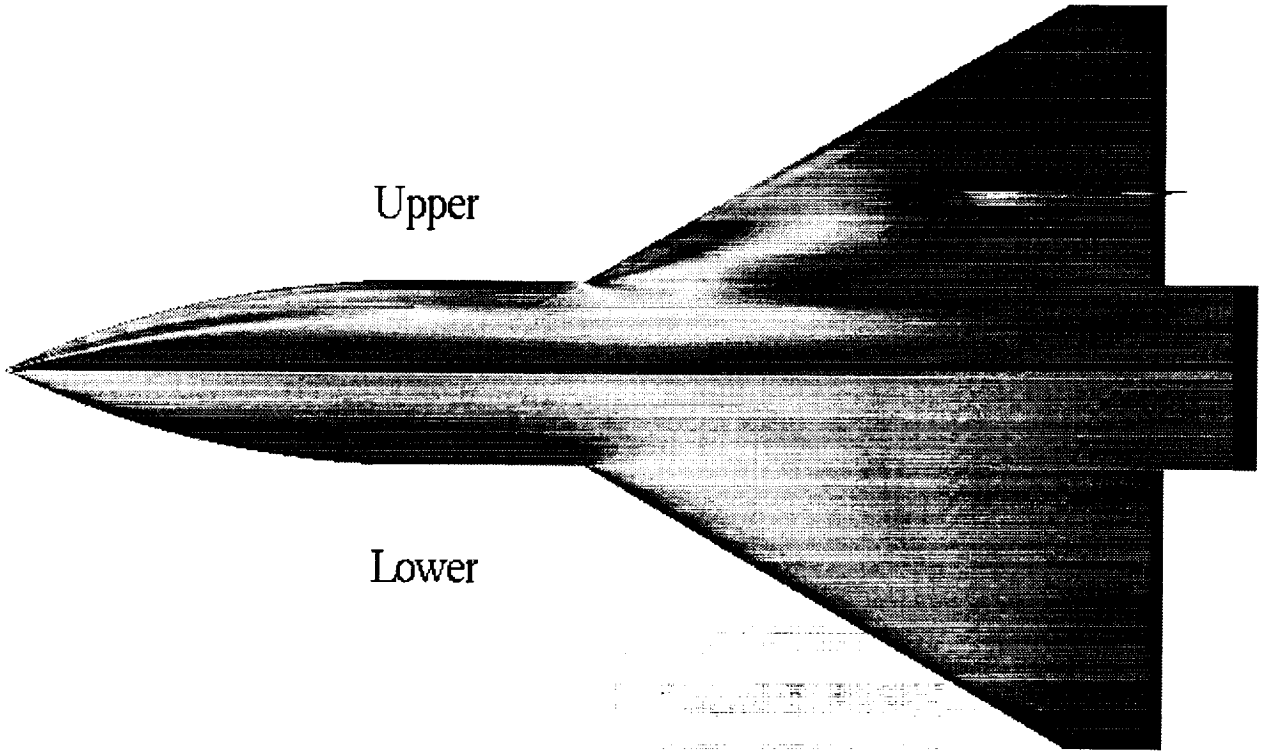

Figure 23. Surface Cp distribution, TEAM RANS viscous solution of burst vortex flow, twin-tail model, M = 0.4, $\alpha = 35.21^{o}$, Re = 2.7 million

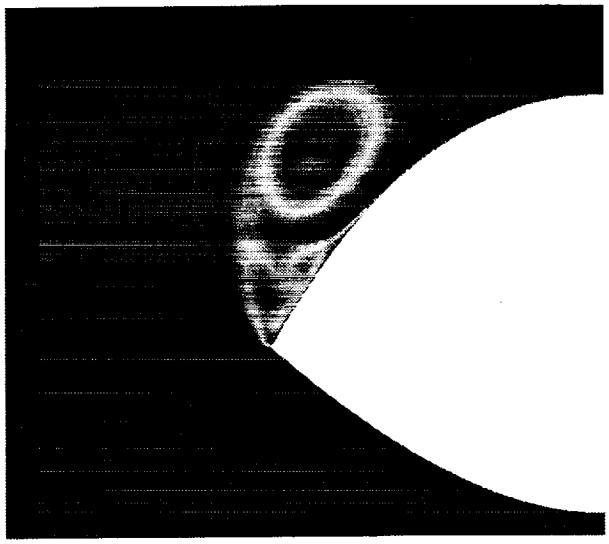

x = 6.11

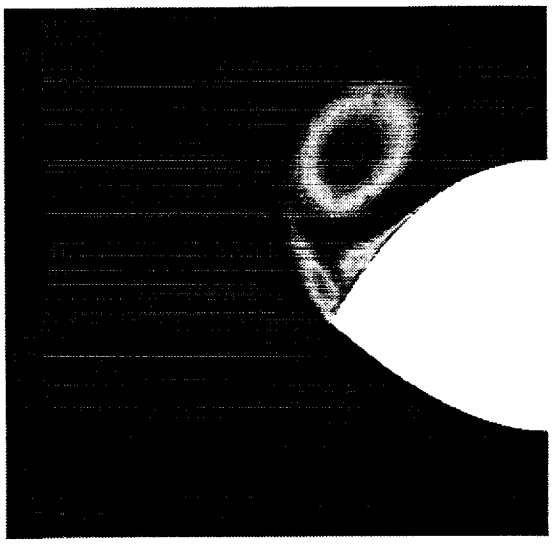

x = 10.45

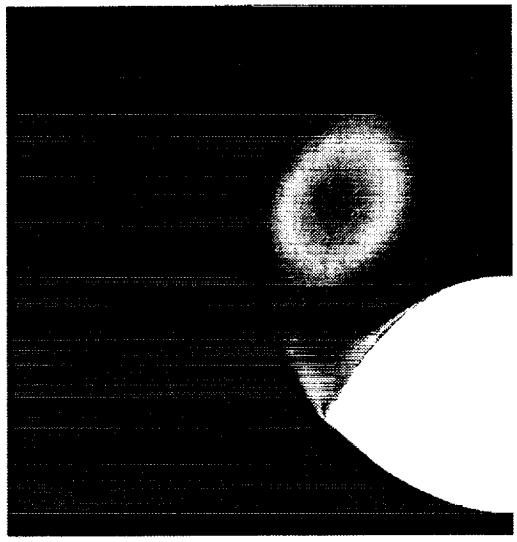

x = 14.5

Figure 24. Off body total pressure distribution at three forebody cross-flow stations, twin-tail model, TEAM RANS viscous analysis, M = 0.4, $\alpha = 35.21^{\circ}$, Re = 2.7 million

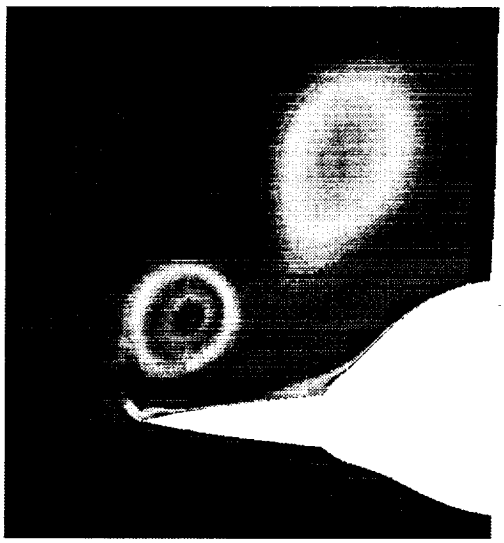

x = 19.05

x = 23.55

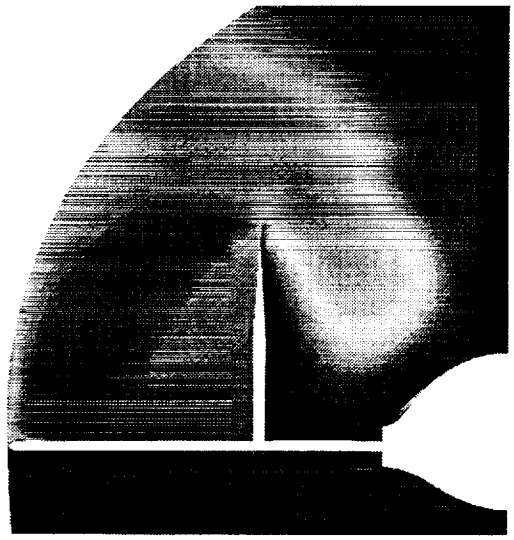

x = 28.05

Figure 25. Off body total pressure distribution at three aft-fuselage and wing stations, twin-tail model, TEAM RANS viscous analysis, M = 0.4, $\alpha = 35.21^{o}$, Re = 2.7 million

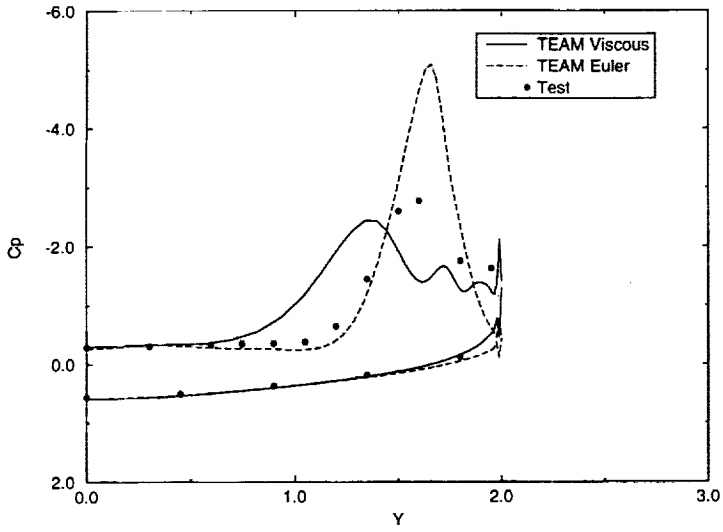

x = 6.11

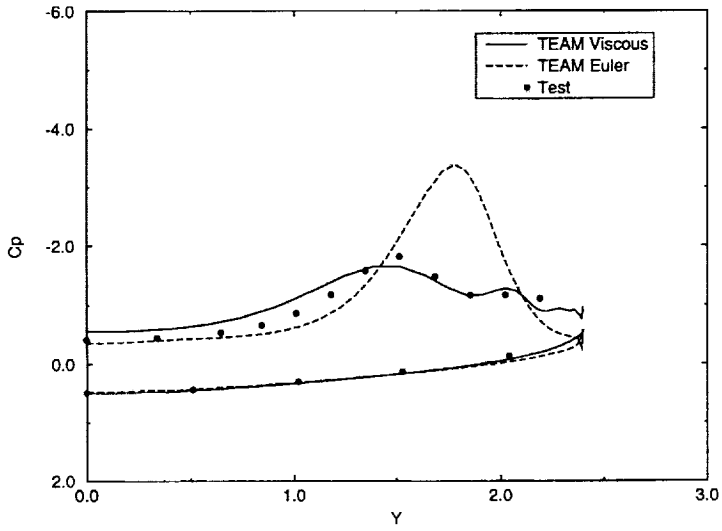

x = 10.45

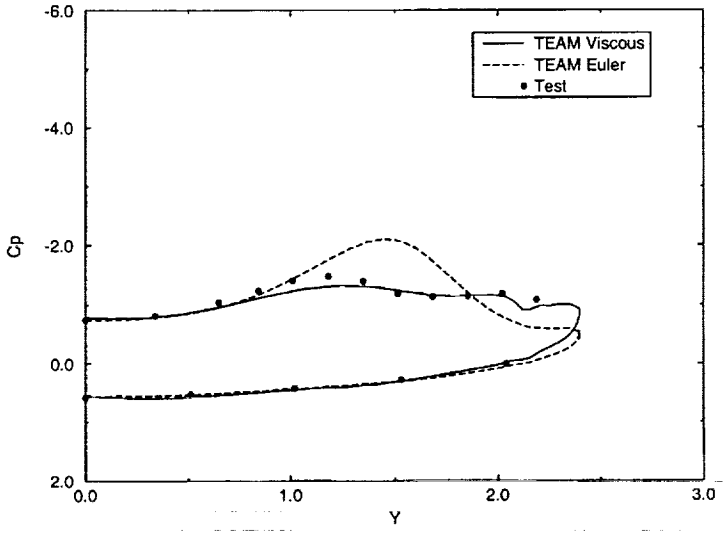

x = 14.5

Figure 26. Viscous effects on surface pressures at the three forebody stations for burst vortex flow, twin-tail model, M = 0.4, $\alpha = 35.21^{o}$, Re = 2.7 million

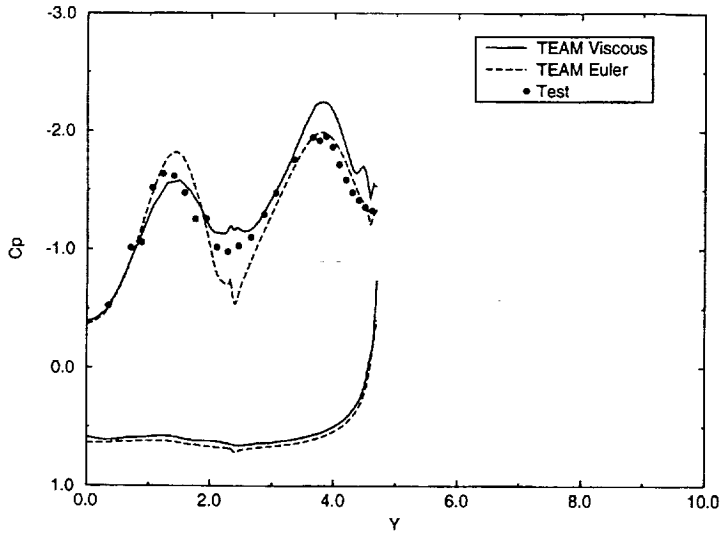

x = 19.05

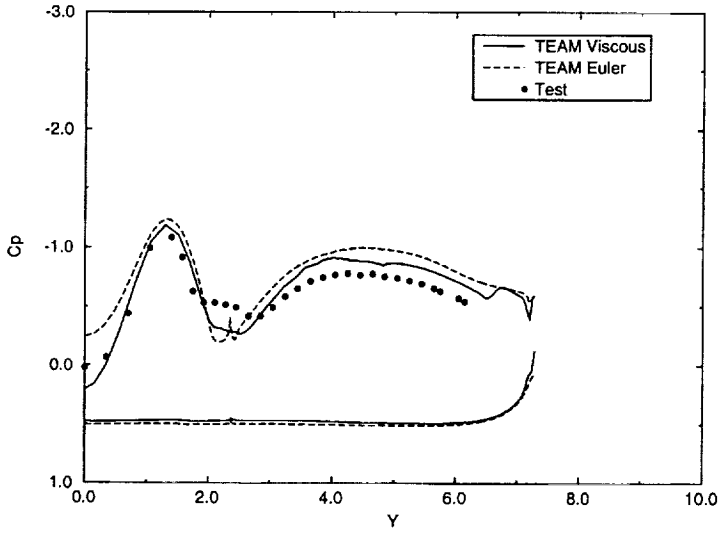

x = 23.55

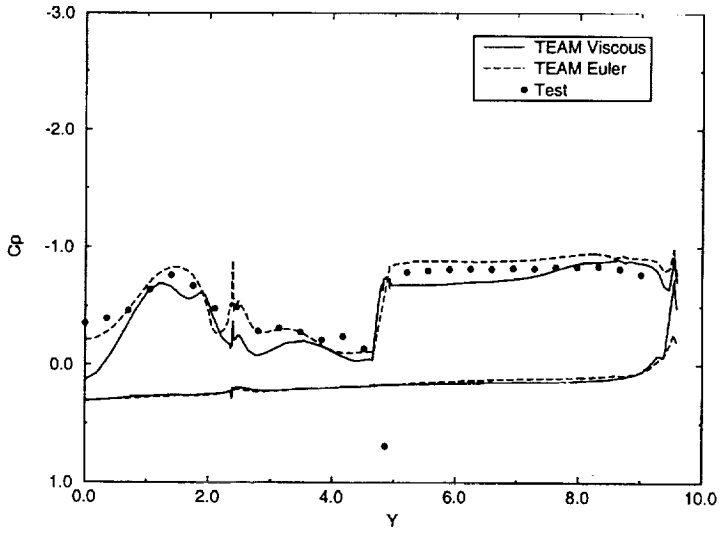

x = 28.05

Figure 27. Viscous effects on surface pressures at the three aft-fuselage and wing stations for burst vortex flow, twin-tail model, M = 0.4, $\alpha = 35.21^{\circ}$, Re = 2.7 million

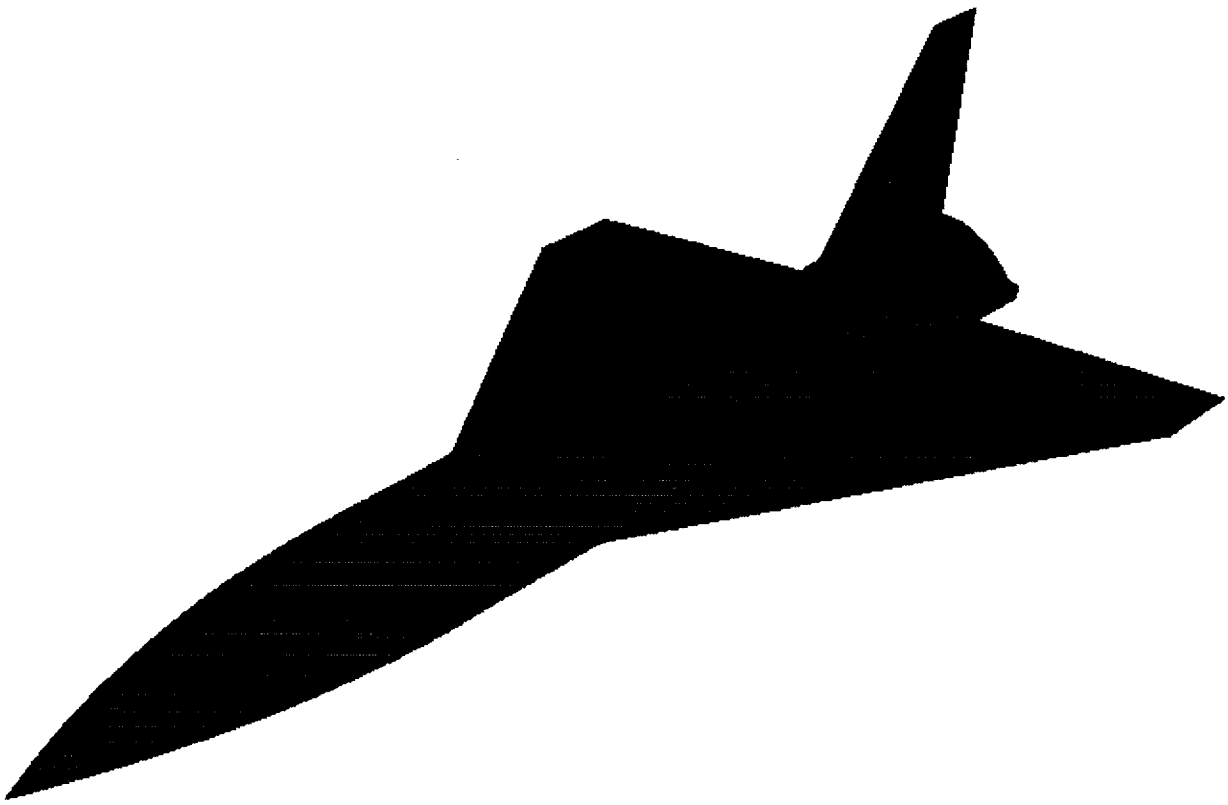

(See figure 1 on page 33 for geometric parameters)

Figure 28. Geometry of MTVI single-tail baseline model

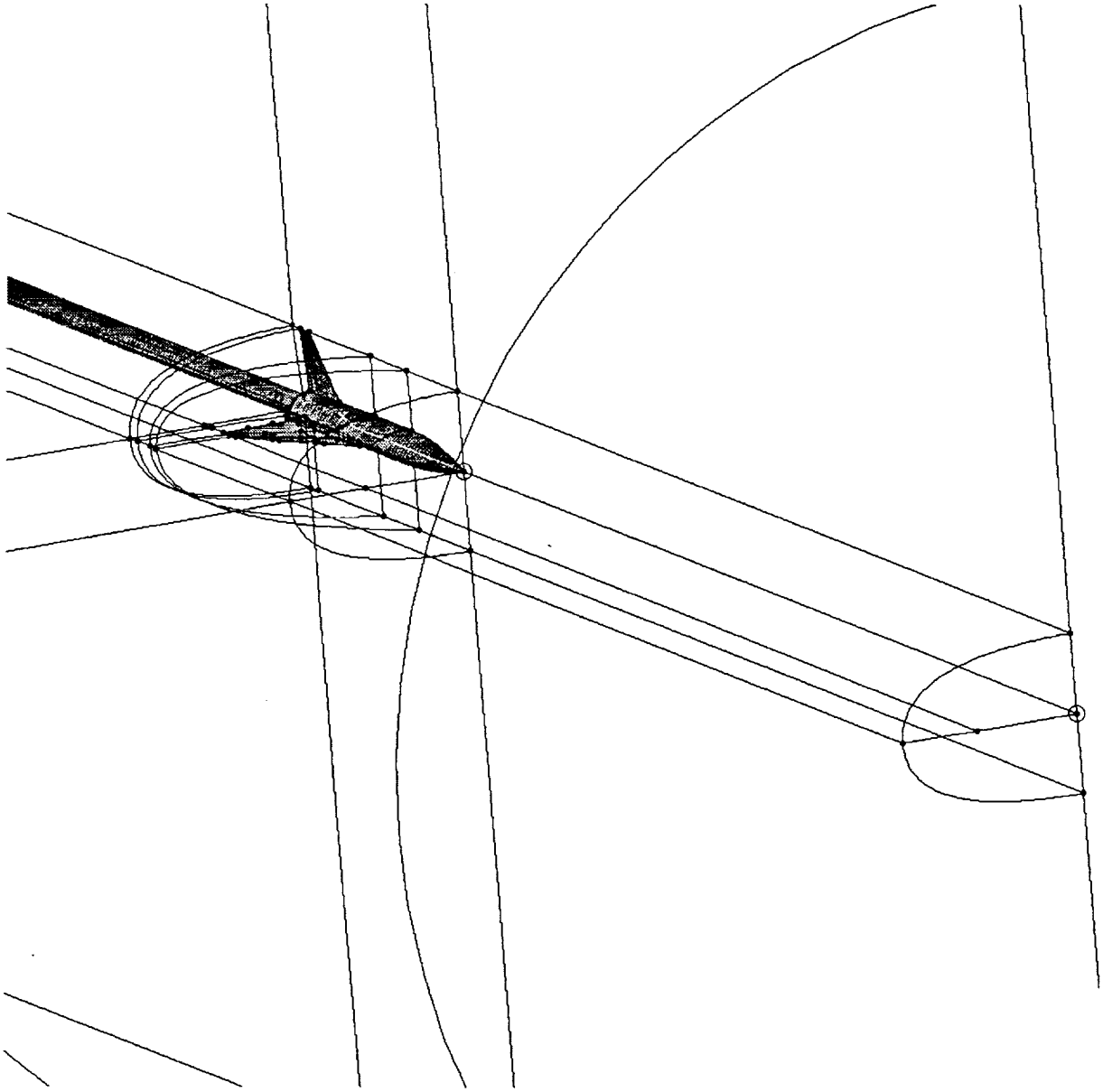

16 Zones

Topology H-H/O-H

Euler: 1,852,668 nodes

Viscous: 2,662,854 nodes

Far Field Locations:

Up-stream: 4 Body Lengths

Down-stream: 5 Body Lengths

Radial: 5 Span Lengths

Grid Generation Time:

Euler: 64 labor-hours

Viscous: 40 additional labor-hours

Figure 29. Grid blocks schematic and grid generation data for single-tail model

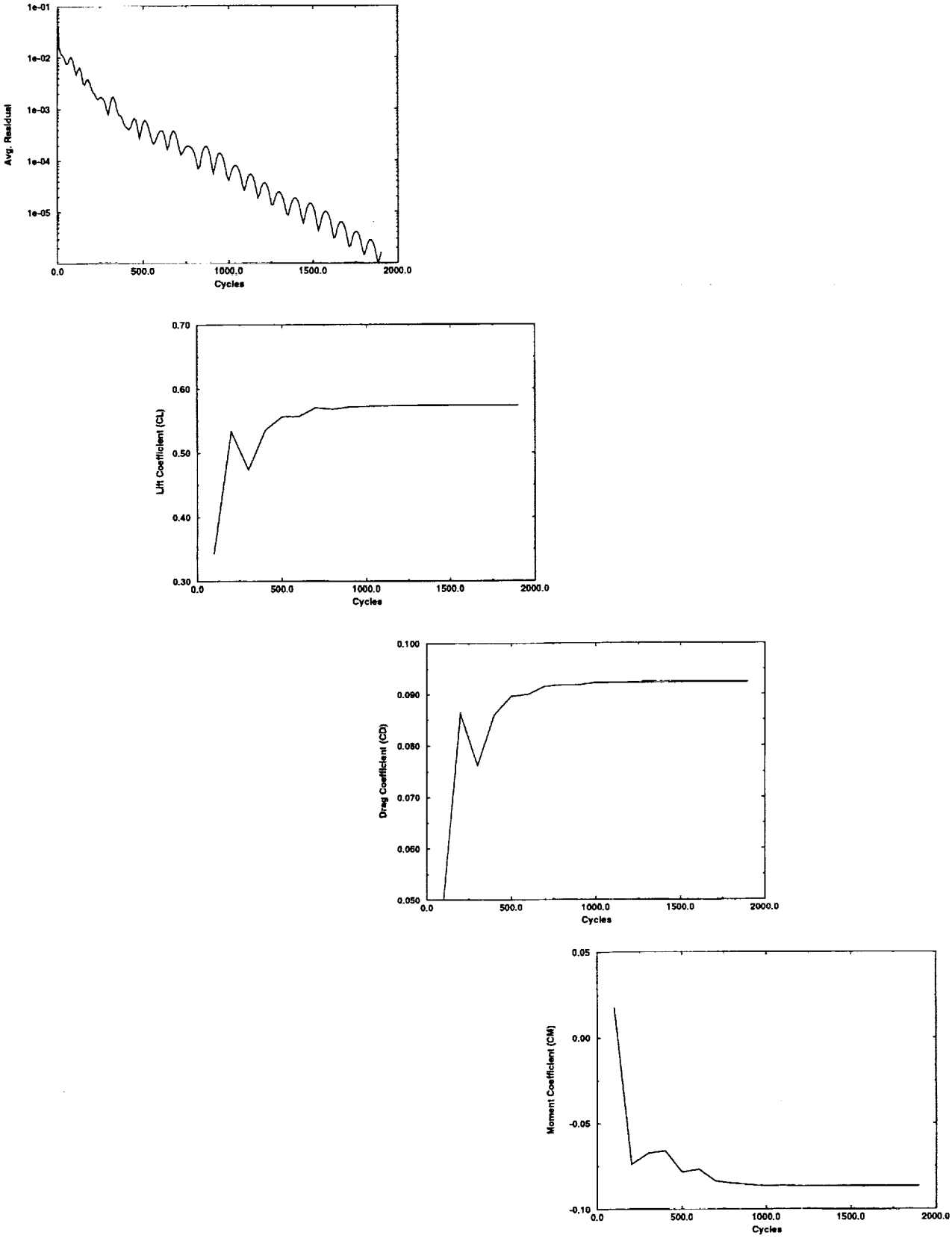

Figure 30. Average residual, lift, drag, and moment convergence histories for TEAM Euler analysis, single-tail model, M = 0.4, $\alpha = 10.1^0$

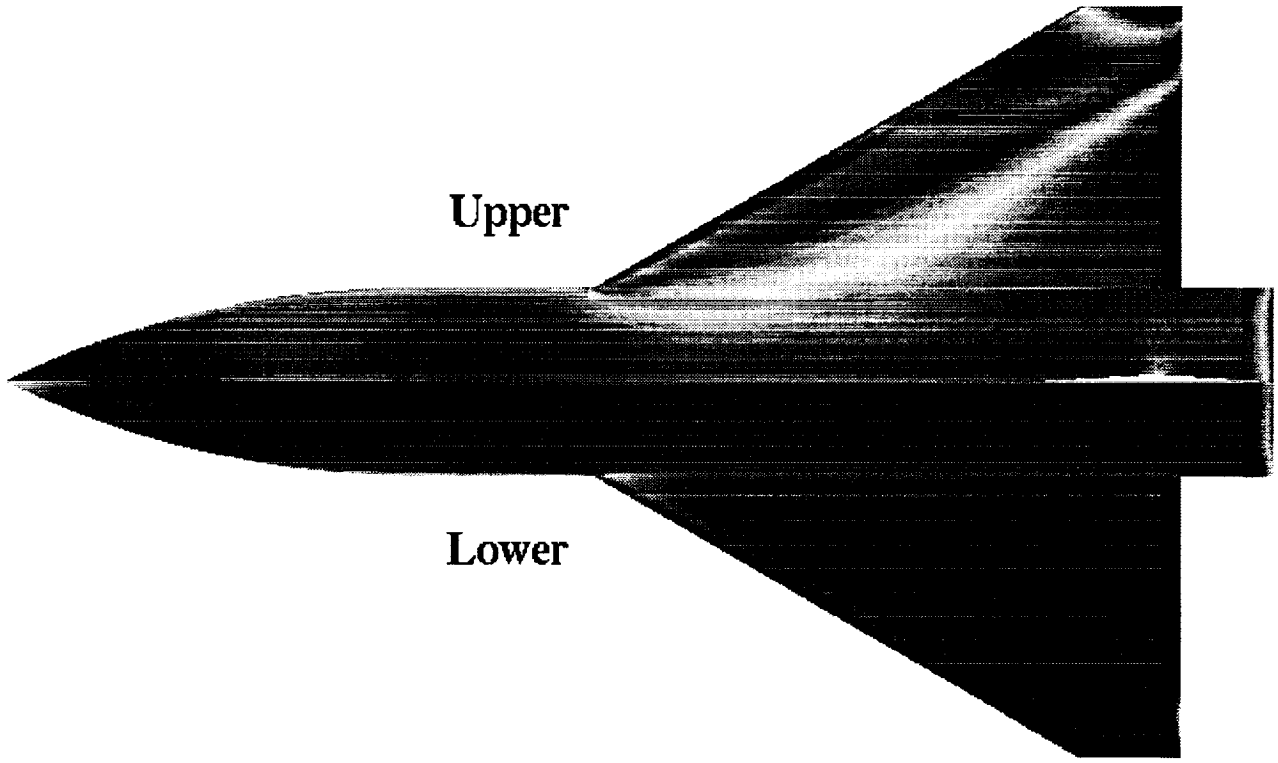

Figure 31. Surface Cp distribution, TEAM Euler solution of benign vortex flow, single-tail model, M = 0.4, α = 10.1°

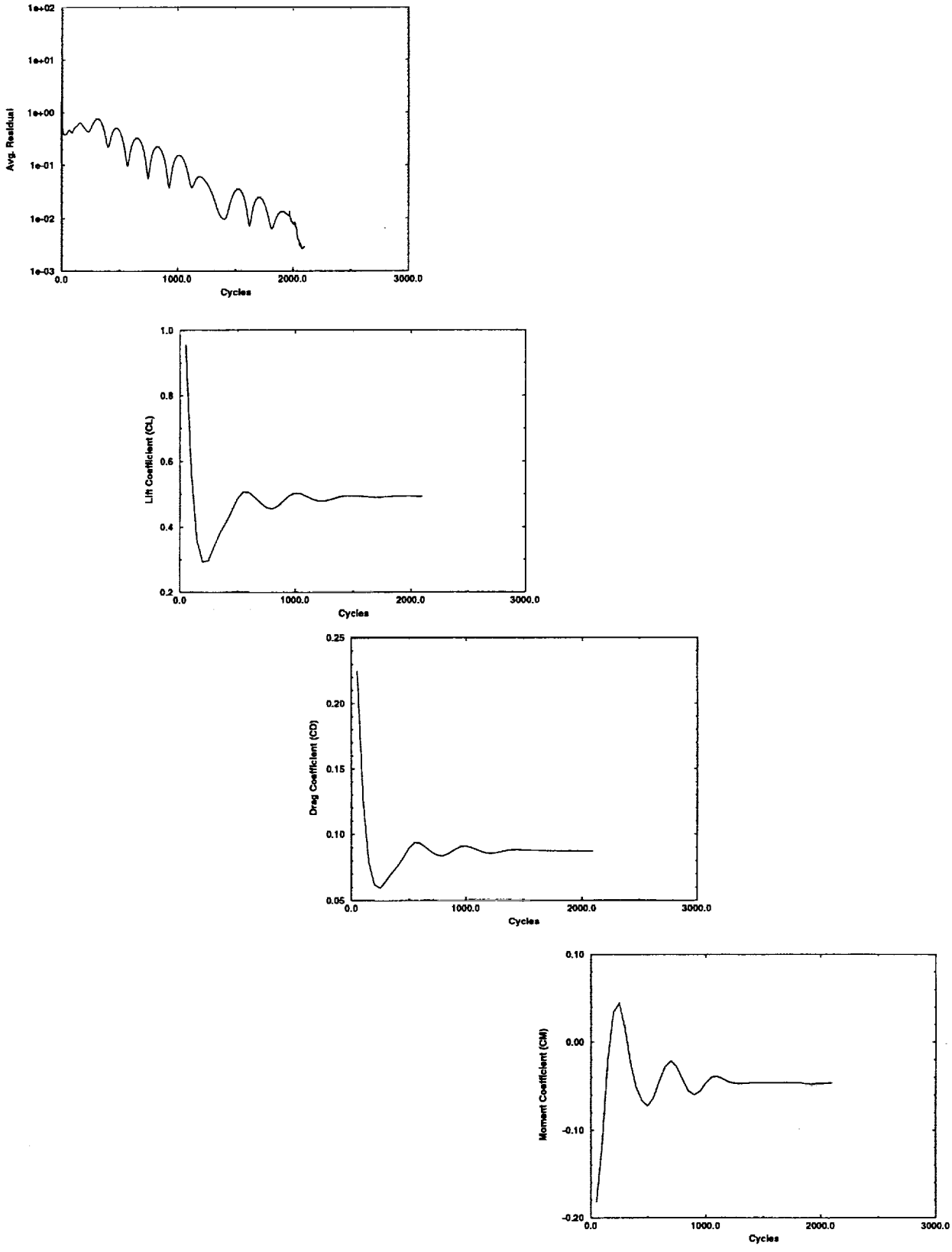

Figure 32. Average residual, lift, drag, and moment convergence histories for TEAM viscous analysis, single-tail model, M = 0.4, α = 10.1°, Re = 2.7 million

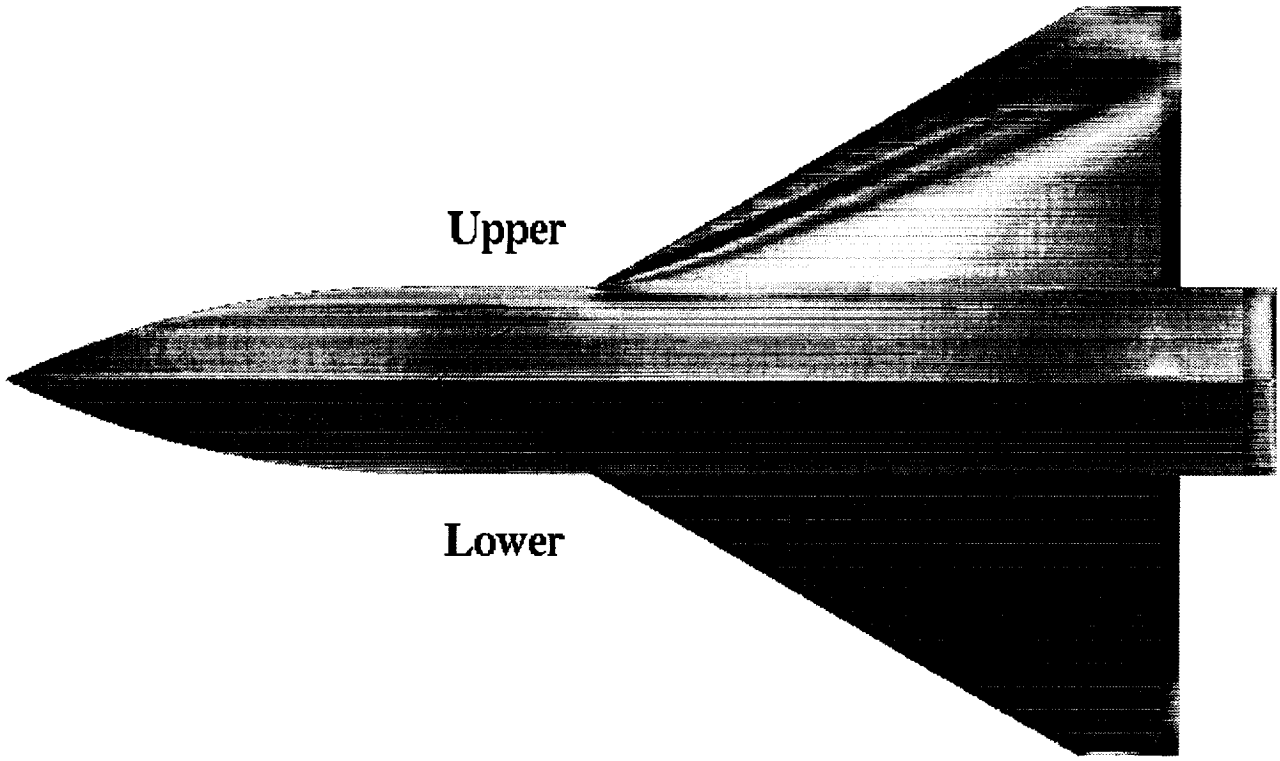

Figure 33. Surface Cp distribution, TEAM RANS viscous solution of benign vortex flow, single-tail MTVI model, M = 0.4, $\alpha = 10.1^{o}$

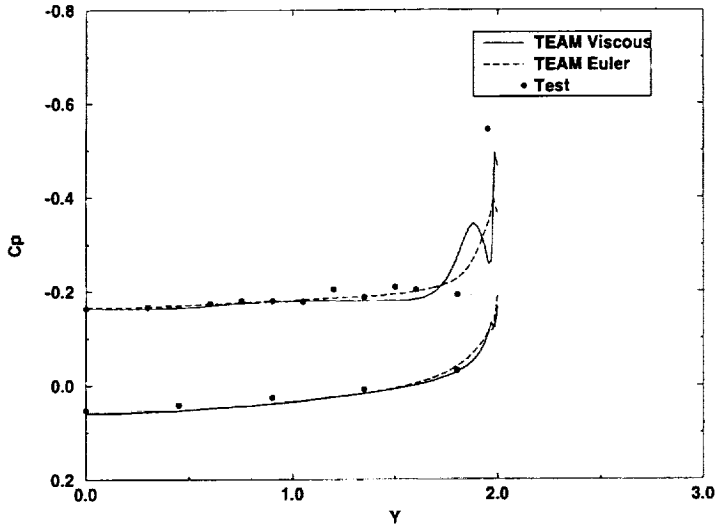

x = 6.11

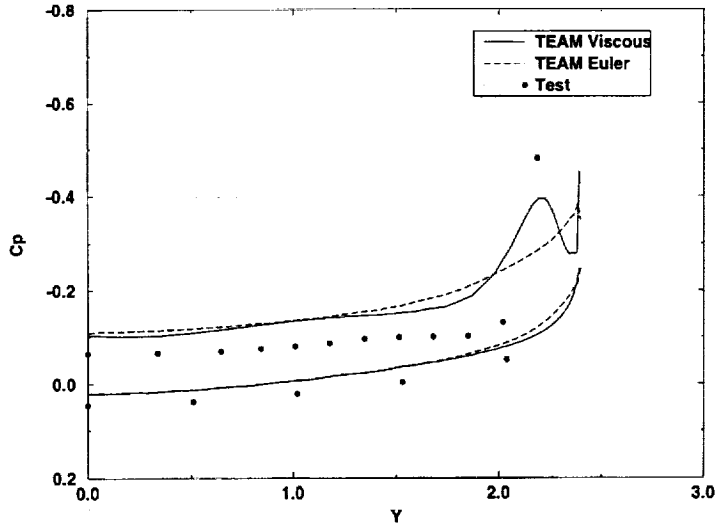

x = 10.45

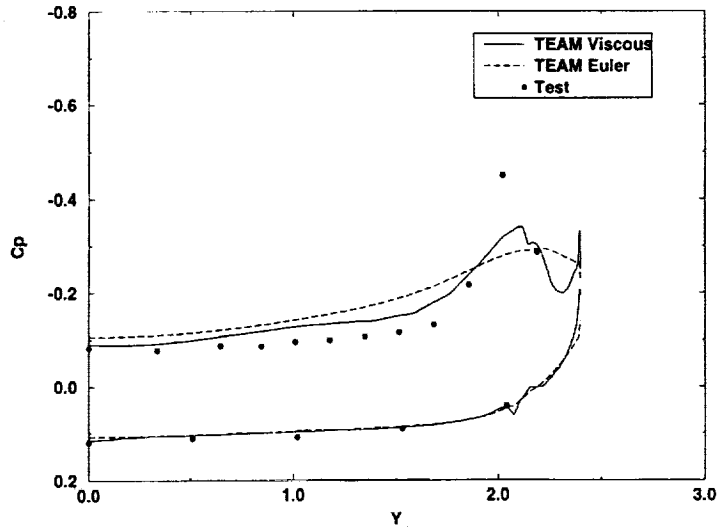

x = 14.5

Figure 34. Viscous effect on surface pressure distribution at the three forebody stations for benign vortex flow, single-tail model, M = 0.4, $\alpha = 10.1^{o}$

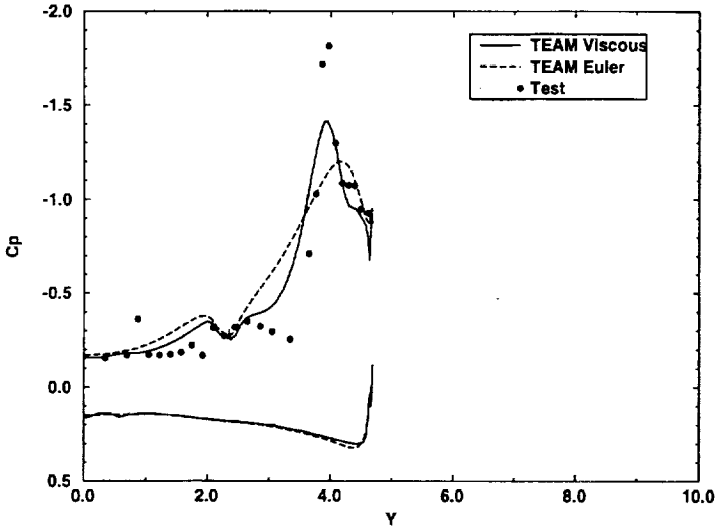

x = 19.05

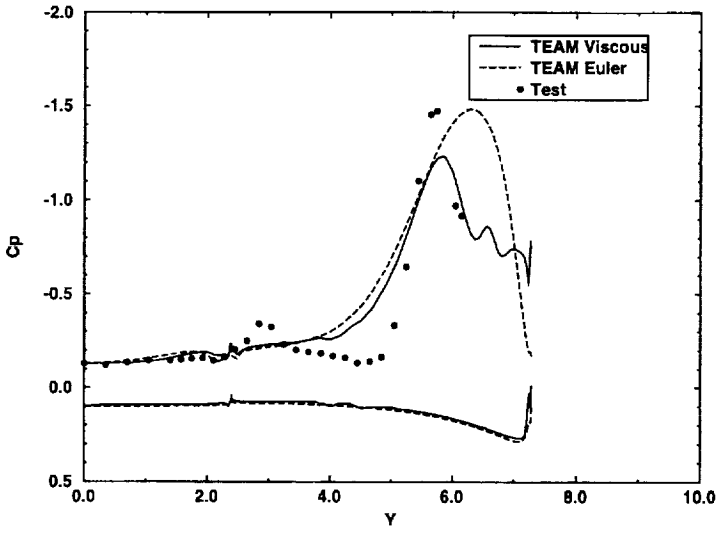

x = 23.55

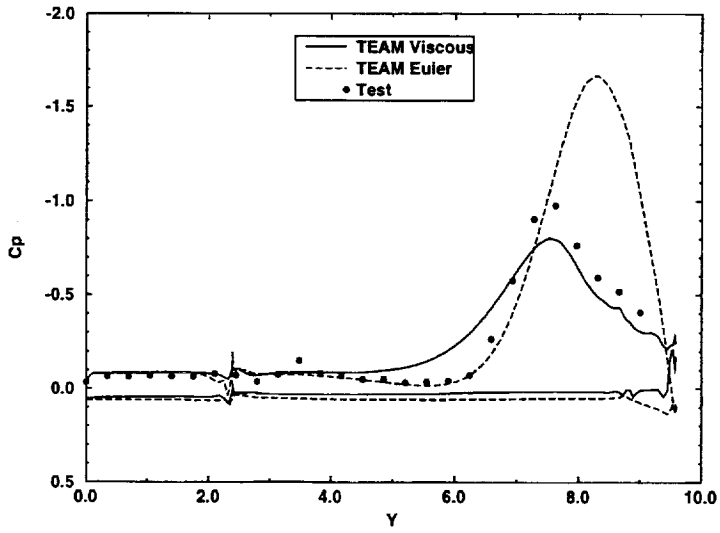

x = 28.05

Figure 35. Viscous effect on surface pressure distribution at the three aft-fuselage and wing stations for benign vortex flow, single-tail model, M = 0.4, $\alpha = 10.1^{o}$

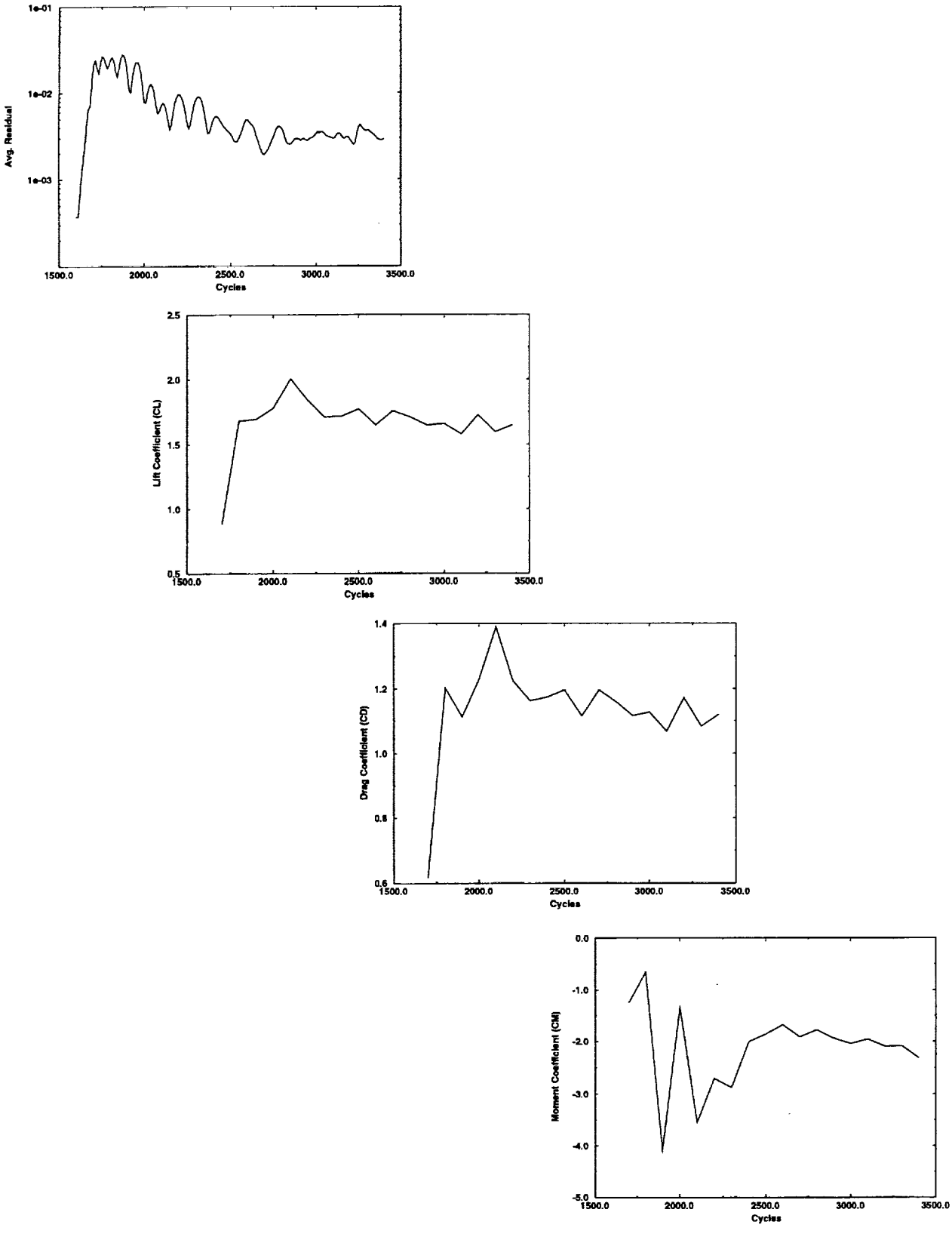

Figure 36. Average residual, lift, drag, and moment convergence histories for TEAM Euler analysis of single-tail model, M = 0.4, $\alpha = 35.35^0$

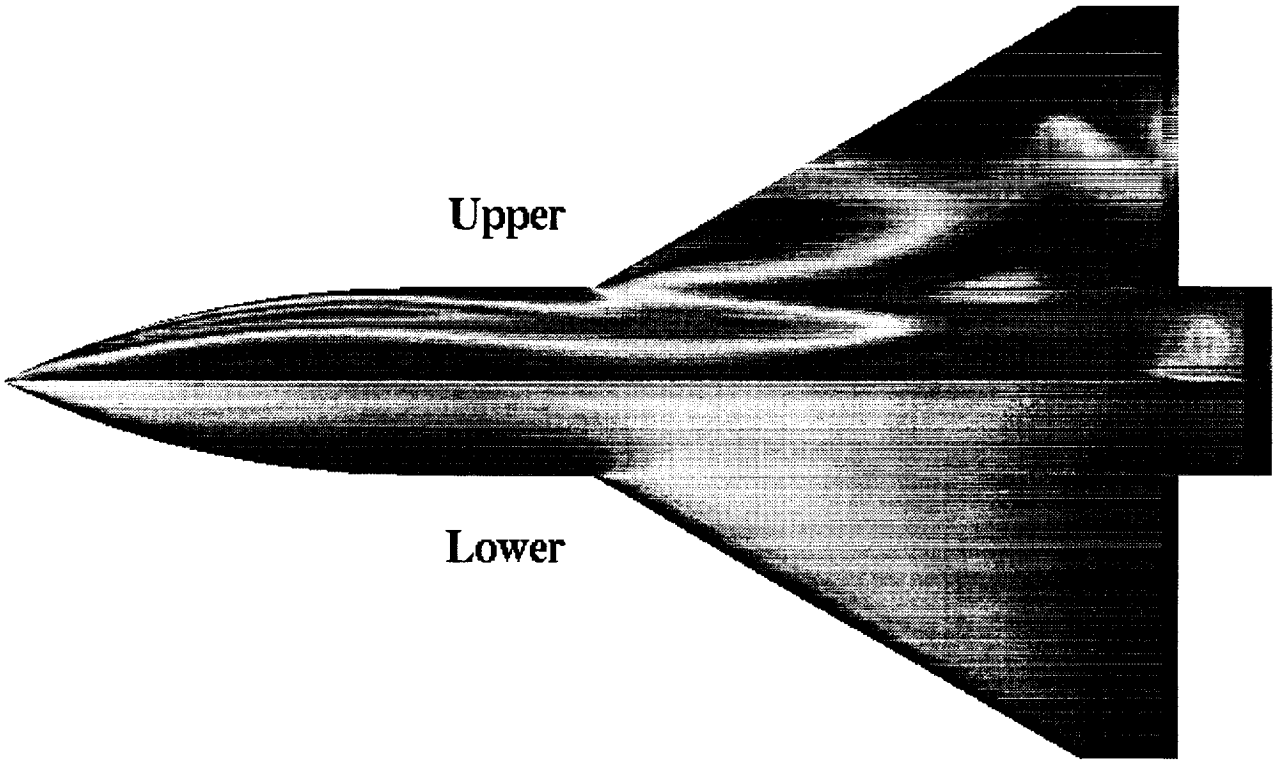

Figure 37. Surface Cp distribution, TEAM Euler solution of burst vortex flow, single tail model, M = 0.4, $\alpha = 35.35^{o}$

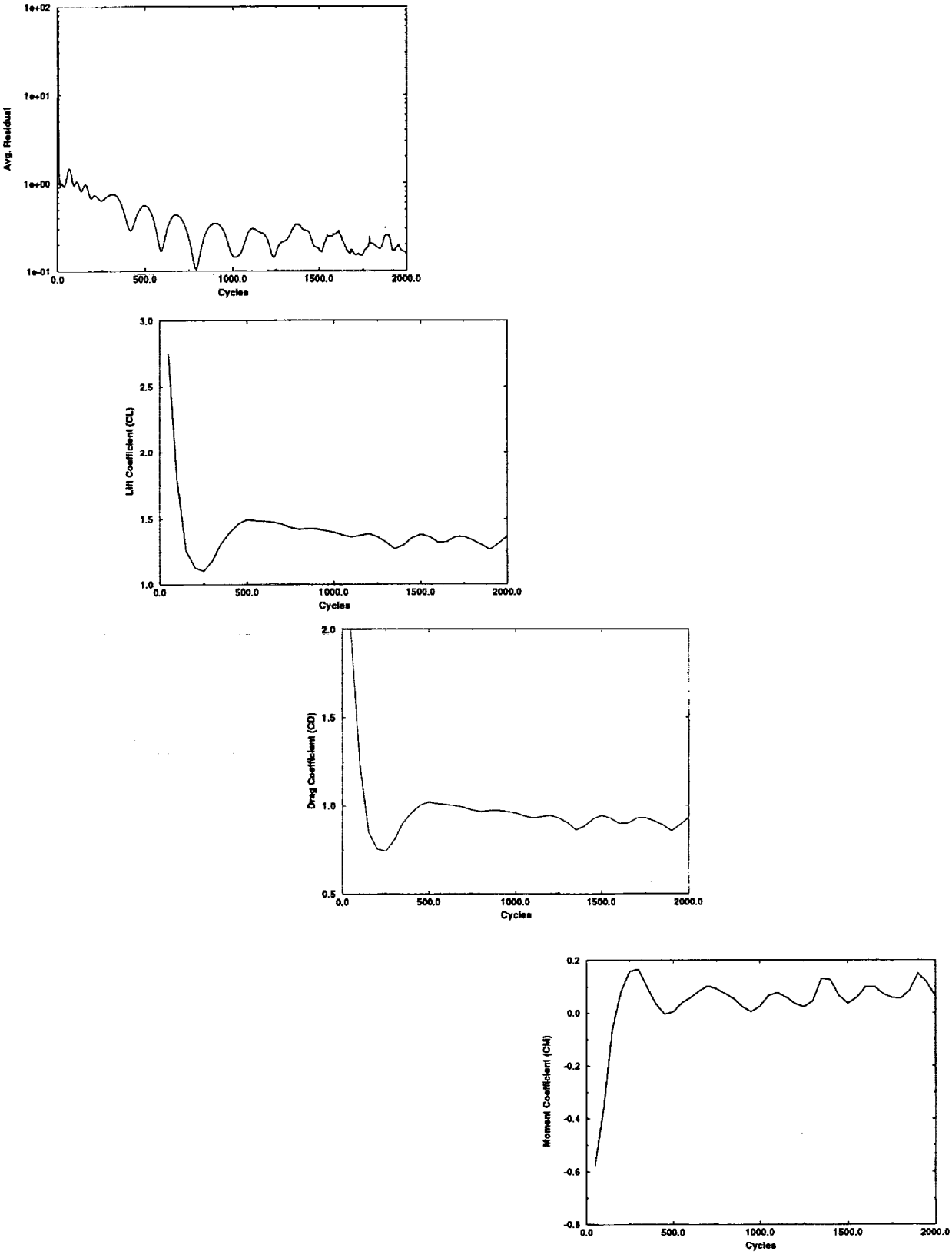

Figure 38. Average residual, lift, drag, and moment convergence histories, single-tail model, TEAM RANS viscous solution, M = 0.4, $\alpha = 35.35^{\circ}$, Re = 2.7 million

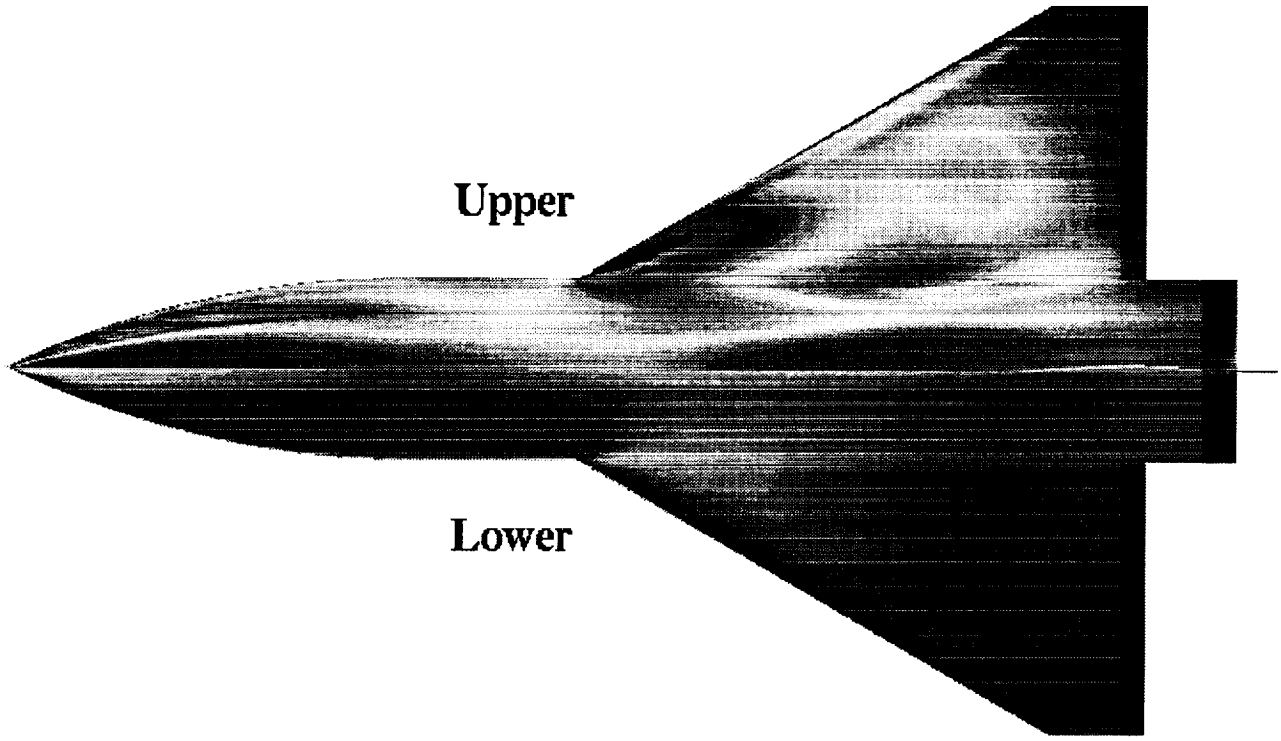

Figure 39. Surface Cp distribution, TEAM RANS viscous solution of burst vortex flow, single tail model, M = 0.4, $\alpha = 35.35^{o}$, Re = 2.7 million

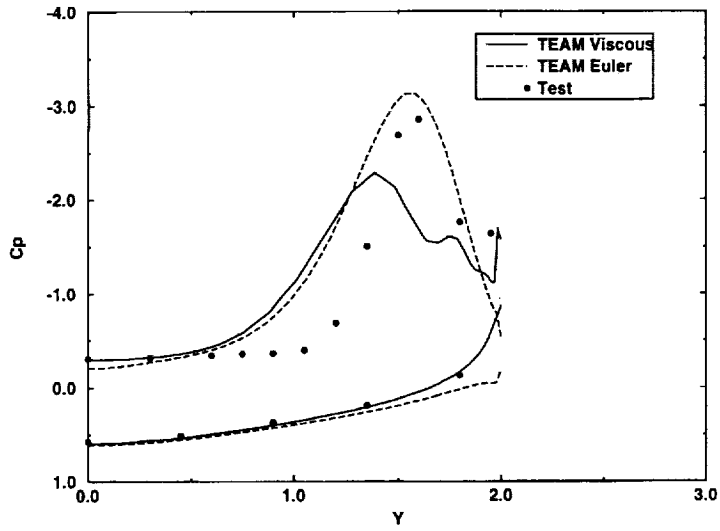

x = 6.11

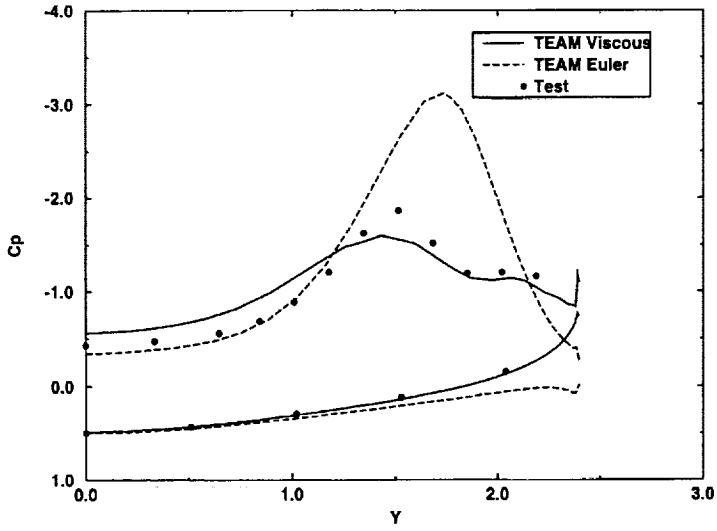

x = 10.45

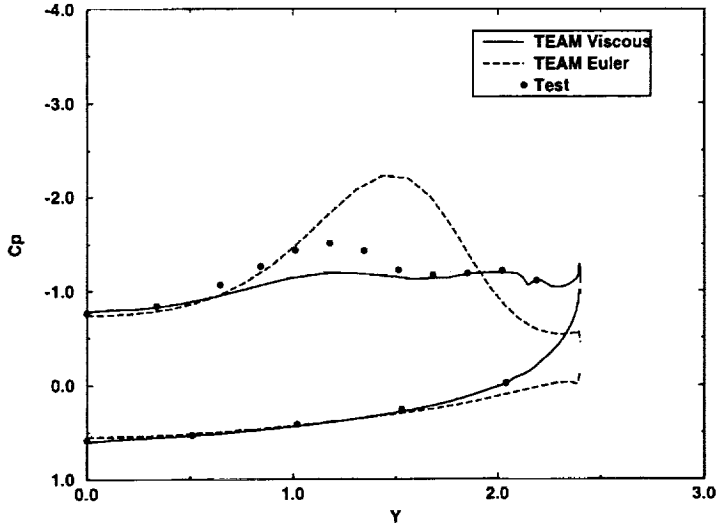

x = 14.5

Figure 40. Viscous effect on surface pressure distribution at the three forebody stations for burst vortex flow, single-tail model, M = 0.4, $\alpha = 35.35^{o}$, Re = 2.7 million

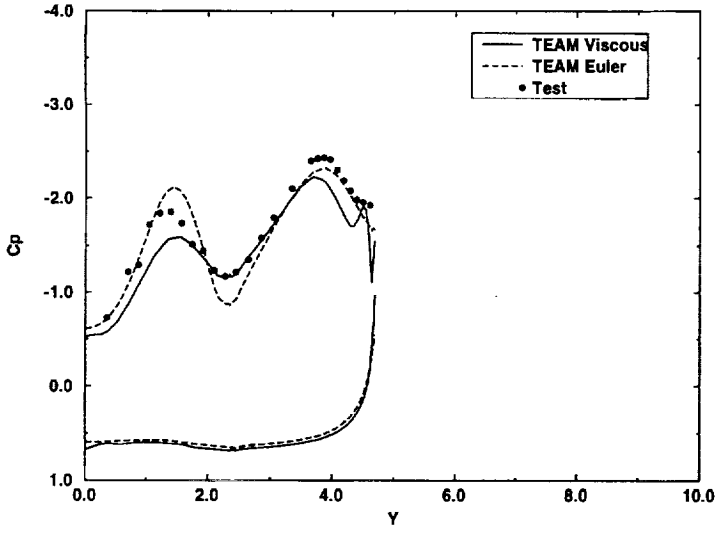

x = 19.05

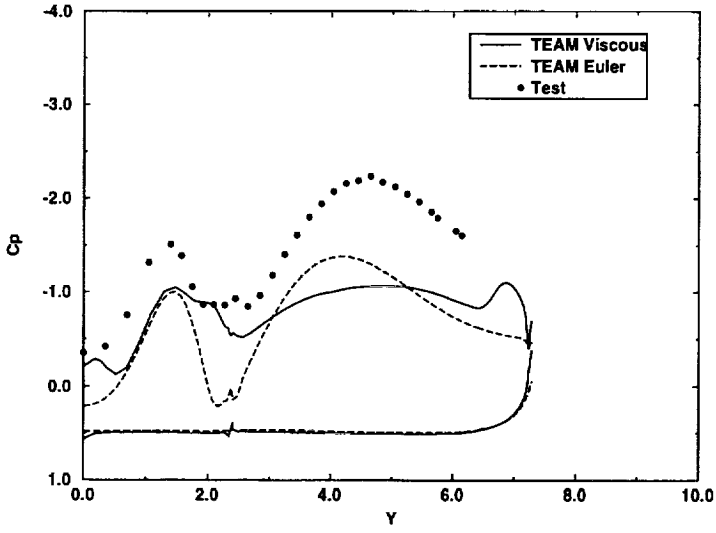

x = 23.55

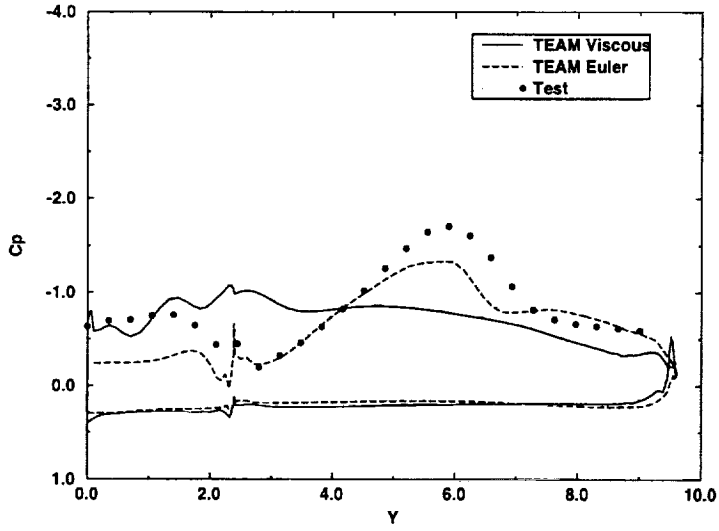

x = 28.05

Figure 41. Viscous effect on surface pressure distribution at the three aft-fuselage and wing stations for burst vortex flow, single-tail model, M = 0.4, $\alpha = 35.35^{o}$, Re = 2.7 million

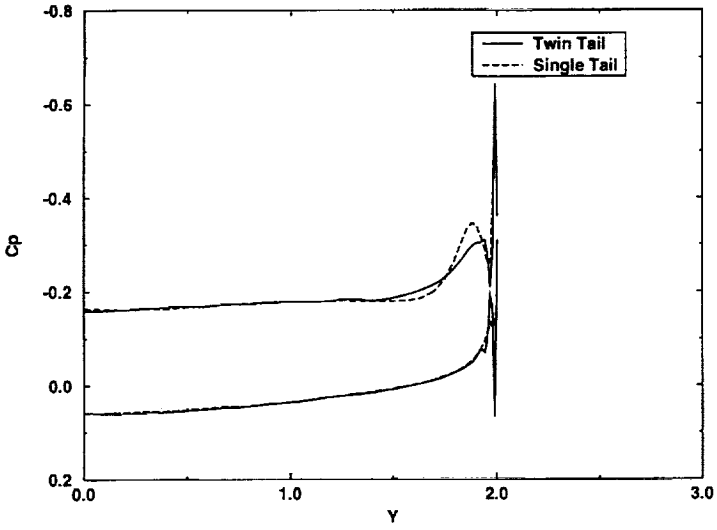

x = 6.11

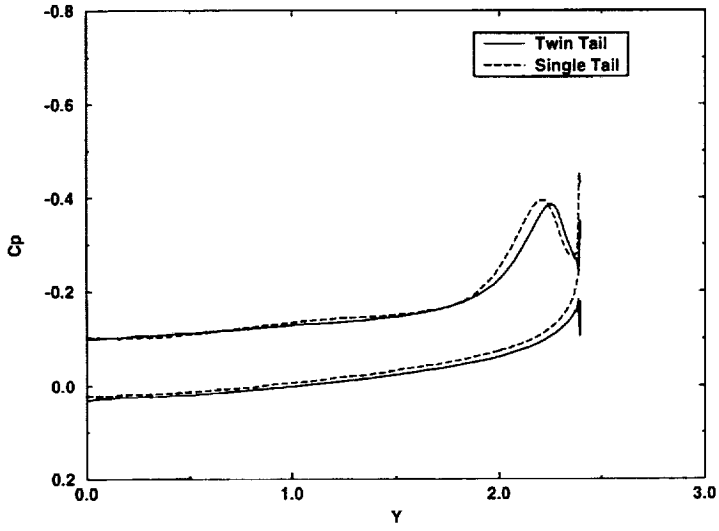

x = 10.45

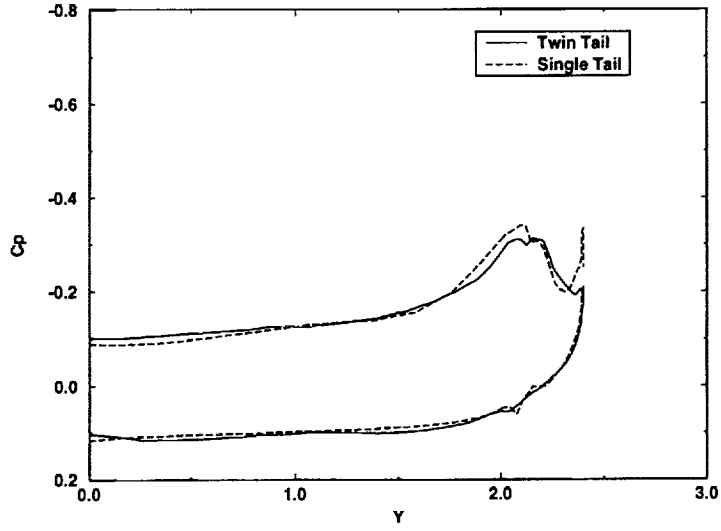

x = 14.5

Figure 42. Effect of tail placement on surface C_p at three forebody stations for benign vortex flow, TEAM RANS viscous solution, M = 0.4, $\alpha = 10.1^{\circ}$, Re = 2.7 million

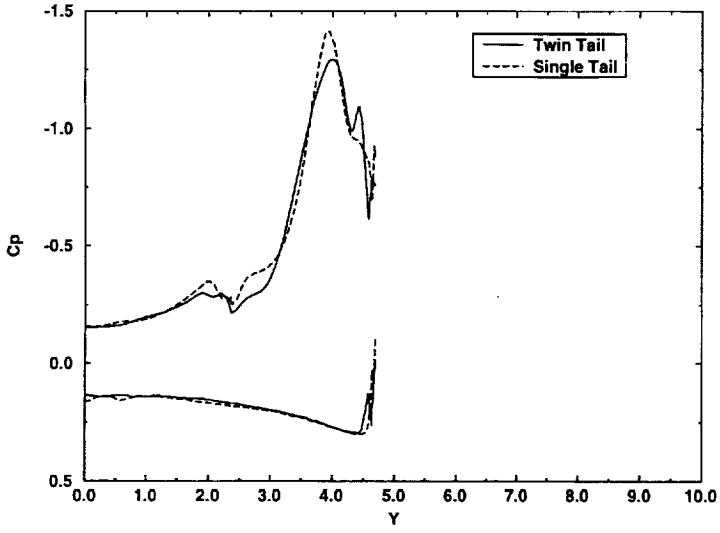

x = 19.05

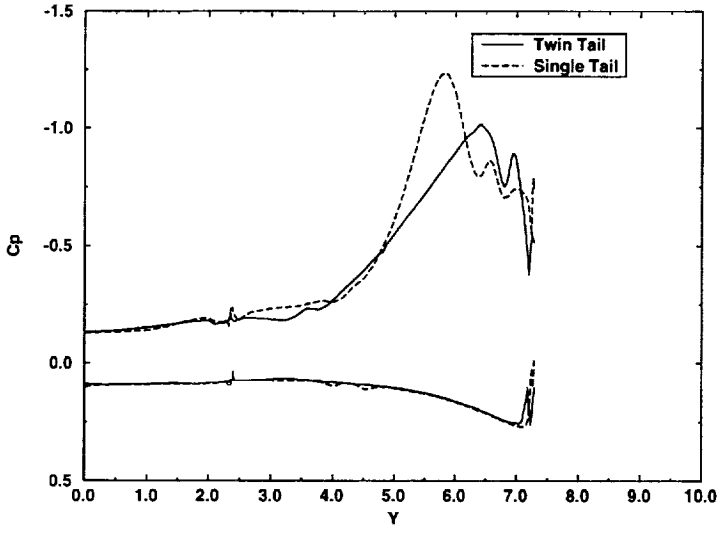

x = 23.55

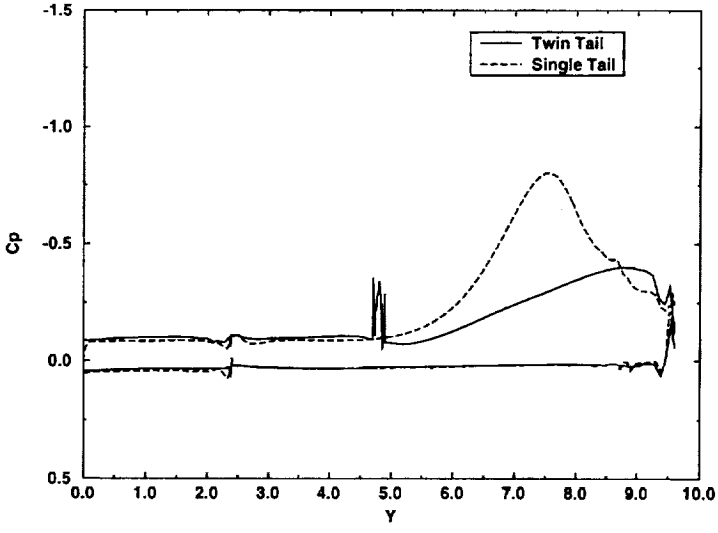

x = 28.05

Figure 43. Effect of tail placement on surface C_p at three aft-fuselage and wing stations for benign vortex flow, TEAM RANS viscous solution, M = 0.4, $\alpha = 10.1^{\circ}$, Re = 2.7 million

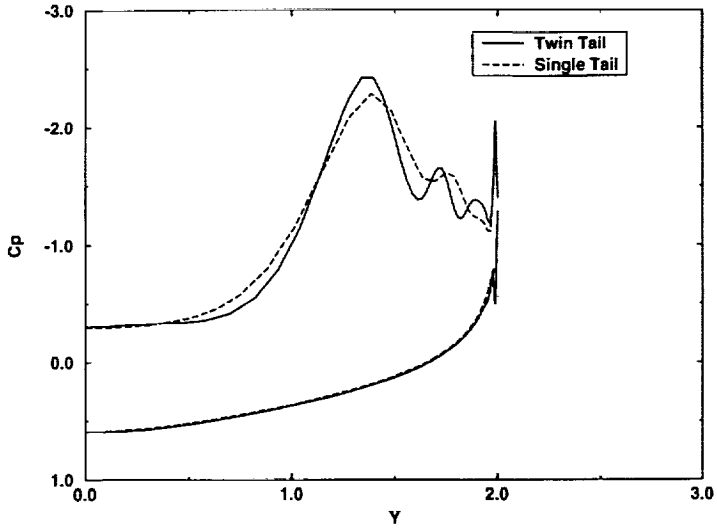

x = 6.11

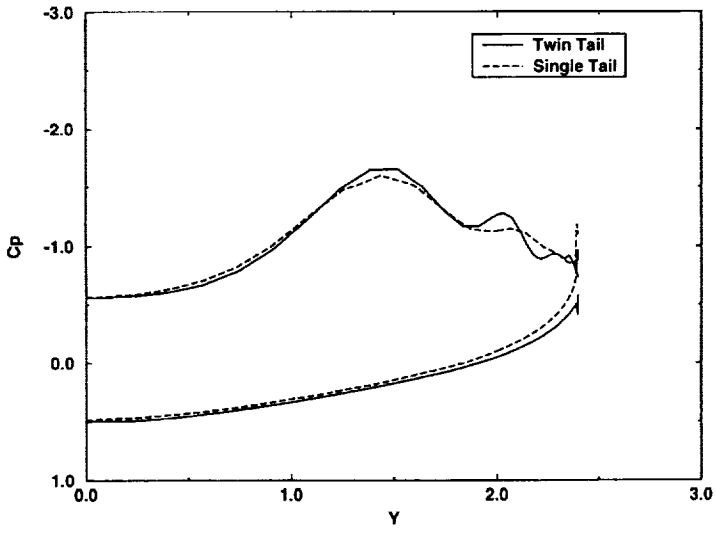

x = 10.45

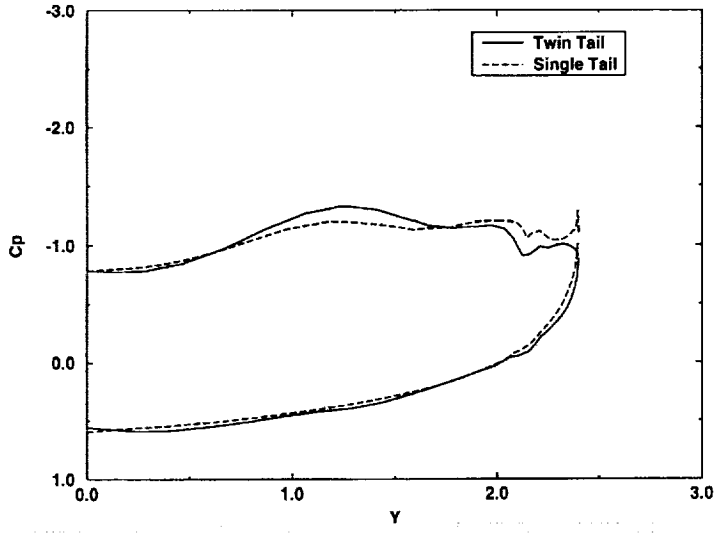

x = 14.5

Figure 44. Effect of tail placement on surface C_p at three forebody stations for burst vortex flow, TEAM RANS viscous solution, M = 0.4, $\alpha = 35^o$, Re = 2.7 million

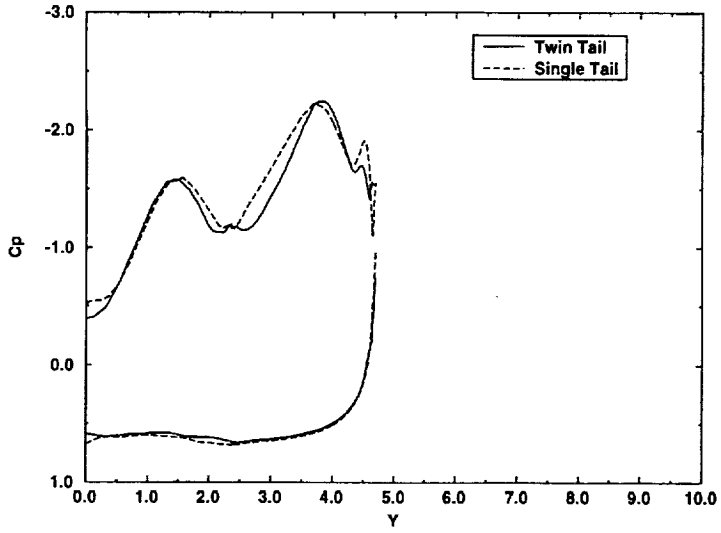

x = 19.05

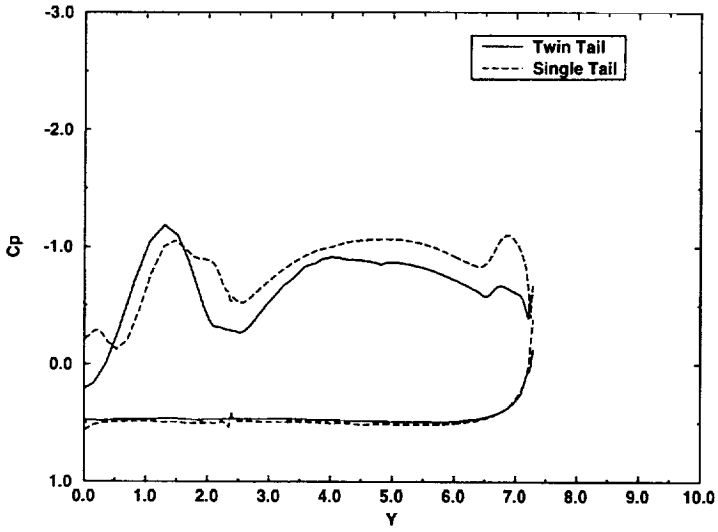

x = 23.55

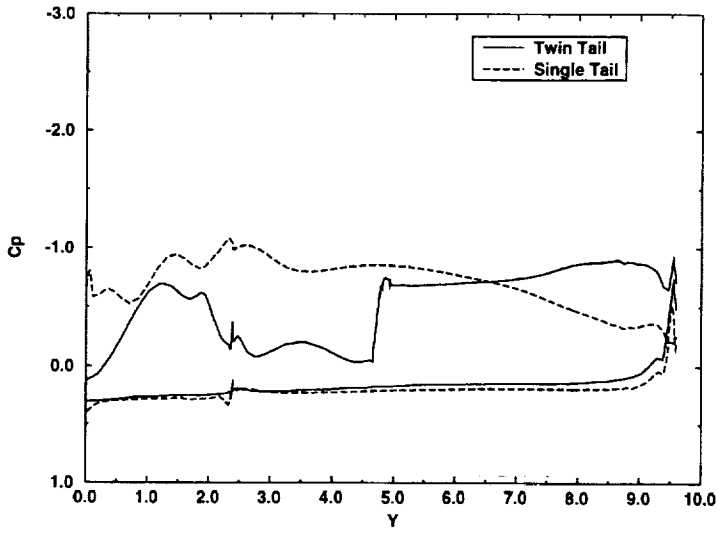

x = 28.05

Figure 45. Effect of tail placement on surface C_p at three aft-fuselage and wing stations for burst vortex flow, TEAM RANS viscous solution, M = 0.4, $\alpha = 35^{\circ}$, Re = 2.7 million

REPORT DOCUMENTATION PAGE

Form Approved
OMB No. 0704-0188

1. AGENCY USE ONLY *(Leave blank)*	2. REPORT DATE	3. REPORT TYPE AND DATES COVERED
	March 1995	Contractor Report (2/1/94 to 8/1/94)

4. TITLE AND SUBTITLE
An Assessment of Viscous Effects in Computational Simulation of Benign and Burst Vortex Flows on Generic Fighter Wind-Tunnel Models Using TEAM Code

5. FUNDING NUMBERS
C NAS1-19000, Task T018
WU 505-68-30-03

6. AUTHOR(S)
Tom A. Kinard, Brenda W. Harris and Pradeep Raj

7. PERFORMING ORGANIZATION NAME(S) AND ADDRESS(ES)
Lockheed Aeronautical Systems Company
Marietta, Georgia 30063

8. PERFORMING ORGANIZATION REPORT NUMBER

9. SPONSORING/MONITORING AGENCY NAME(S) AND ADDRESS(ES)
National Aeronautics and Space Administration
Langley Research Center
Hampton, VA 23681-0001

10. SPONSORING/MONITORING AGENCY REPORT NUMBER
NASA CR-4650

11. SUPPLEMENTARY NOTES
Technical Monitor: Mr. Farhad Ghaffari
NASA Langley Research Center
Hampton VA 23681-0001

12a. DISTRIBUTION/AVAILABILITY STATEMENT
Unclassified-Unlimited
Subject Category 02

12b. DISTRIBUTION CODE

13. ABSTRACT *(Maximum 200 words)*

Vortex flows on a twin-tail and a single-tail modular transonic vortex interaction (MTVI) model, representative of a generic fighter configuration, are computationally simulated in this study using the Three-dimensional Euler/Navier-Stokes Aerodynamic Method (TEAM). The primary objective is to provide an assessment of viscous effects on benign (10° angle of attack) and burst (35° angle of attack) vortex flow solutions. This study was conducted in support of a NASA project aimed at assessing the viability of using Euler technology to predict aerodynamic characteristics of aircraft configurations at moderate-to-high angles of attack in a preliminary design environment. The TEAM code solves the Euler and Reynolds-average Navier-Stokes equations on patched multiblock structured grids. Its algorithm is based on a cell-centered finite-volume formulation with multistage time-stepping scheme. Viscous effects are assessed by comparing the computed inviscid and viscous solutions with each other and experimental data. Also, results of Euler solution sensitivity to grid density and numerical dissipation are presented for the twin-tail model. The results show that proper accounting of viscous effects is necessary for detailed design and optimization but Euler solutions can provide meaningful guidelines for preliminary design of flight vehicles which exhibit vortex flows in parts of their flight envelope.

14. SUBJECT TERMS
Computational Fluid Dynamics, Euler/Navier-Stokes formulation, Sharp-edge flow separation, Viscous effects, Vortex burst, TEAM

15. NUMBER OF PAGES
82

16. PRICE CODE
A05

17. SECURITY CLASSIFICATION OF REPORT	18. SECURITY CLASSIFICATION OF THIS PAGE	19. SECURITY CLASSIFICATION OF ABSTRACT	20. LIMITATION OF ABSTRACT
Unclassified	Unclassified	Unclassified	

National Aeronautics and
Space Administration
Langley Research Center
Mail Code 180
Hampton, VA 23681-00001